ARTICLE OPEN

Check for updates

Prefrontal parvalbumin interneurons mediate CRHR1-dependent early-life stress-induced cognitive deficits in adolescent male mice

Yu-Nu Ma[1], Chao-Juan Yang[2], Chen-Chen Zhang[1], Ya-Xin Sun[1], Xing-Duo Yao[1], Xiao Liu[1], Xue-Xin Li[1], Hong-Li Wang[1], Han Wang[1], Ting Wang[1], Xiao-Dong Wang[3], Chen Zhang[4], Yun-Ai Su[1✉], Ji-Tao Li[1✉] and Tian-Mei Si[1✉]

Cognitive impairment, a core symptom of psychiatric disorders, is frequently observed in adolescents exposed to early-life stress (ES). However, the underlying neural mechanisms are unclear, and therapeutic efficacy is limited. Targeting parvalbumin-expressing interneurons (PVIs) in the medial prefrontal cortex (mPFC), we report that ES reduces mPFC PVI activity, which causally mediated ES-induced cognitive deficits in adolescent male mice through chemogenetic and optogenetic experiments. To understand the possible causes of PVI activity reduction following ES, we then demonstrated that ES upregulated corticotropin-releasing hormone (CRH) receptor 1 [CRHR1, mainly expressed in pyramidal neurons (PNs)] and reduced activity of local pyramidal neurons (PNs) and their excitatory inputs to PVIs. The subsequent genetic manipulation experiments (CRHR1 knockout, CRH overexpression, and chemogenetics) highlight that ES-induced PVI activity reduction may result from CRHR1 upregulation and PN activity downregulation and that PVIs play indispensable roles in CRHR1- or PN-mediated cognitive deficits induced by ES. These results suggest that ES-induced cognitive deficits could be attributed to the prefrontal CRHR1-PN-PVI pathway. Finally, treatment with antalarmin (a CRHR1 antagonist) and environmental enrichment successfully restored the PVI activity and cognitive deficits induced by ES. These findings reveal the neurobiological mechanisms underlying ES-induced cognitive deficits in adolescent male mice and highlight the therapeutic potentials of PVIs in stress-related cognitive deficits in adolescent individuals.

Molecular Psychiatry (2025) 30:2407–2426; https://doi.org/10.1038/s41380-024-02845-6

INTRODUCTION

The first episodes of several psychiatric disorders often occur in adolescence, and this phenomenon is associated with various genetic and environmental risk factors [1, 2]. One such risk factor is early-life stress (ES). Meta-analyses have shown that exposure to adverse life events increases the diagnosis of depression in childhood or adolescence by approximately 2.5 times [3]. Cognitive impairment is one of the core symptoms of several psychiatric disorders and is frequently observed in adolescents exposed to ES [4]. However, the neural mechanisms underlying cognitive impairment remain unclear and the efficacy of current first-line therapeutic drugs for cognitive deficits is limited [5, 6]. Importantly, several recent studies have provided behavioral evidence that ES can significantly impair cognition in adolescent animals [7–9], paving the way for identifying potential neural correlates for early and effective interventions.

The prefrontal cortex (PFC) plays crucial roles in cognitive behaviors, is a late-developing neural structure, and is highly vulnerable to ES [10, 11]. Within the PFC, parvalbumin-expressing interneurons (PVIs) are the largest class of inhibitory neurons (accounting for approximately 40% of interneurons) [12]. They form perisomatic projections onto excitatory pyramidal neurons (PNs), control neural network synchrony, and are crucial for learning and memory [13–15]. Genetic manipulations to inactivate [16, 17] or activate [18, 19] PVIs in the medial PFC (mPFC) have supported the causal link between PVI activity and mPFC-dependent cognitive abilities in adult animals. During adolescence, PVIs undergo a protracted period of maturation and their maturation contributes significantly to the stability of cortical excitatory-inhibitory microcircuits [20] and the development of PFC-dependent cognitive abilities [21, 22]. For instance, sustained inhibition of the mPFC PVI activity in adolescent mice was found to disrupt cognitive flexibility in adulthood [18]. To date, only a few studies have examined the effects of ES on PVIs in adolescents, and largely focused on the number (density) of PVIs [9, 23–25]. Whether and how ES would affect the activity of PFC PVIs in adolescence and how this alteration is linked to ES-induced cognitive deficits remain unknown. Moreover, several mechanisms

[1]Peking University Sixth Hospital, Peking University Institute of Mental Health, NHC Key Laboratory of Mental Health (Peking University), National Clinical Research Center for Mental Disorders (Peking University Sixth Hospital), Beijing, China. [2]Key Laboratory of Biomechanics and Mechanobiology (Beihang University), Ministry of Education, Beijing Advanced Innovation Center for Biomedical Engineering, School of Engineering Medicine, Beihang University, Beijing, China. [3]Department of Neurobiology, Key Laboratory of Medical Neurobiology of Ministry of Health of China, Zhejiang Province Key Laboratory of Neurobiology, Zhejiang University School of Medicine, Hangzhou, China. [4]Department of Neurobiology, School of Basic Medical Sciences, Beijing Key Laboratory of Neural Regeneration and Repair, Advanced Innovation Center for Human Brain Protection, Capital Medical University, Beijing, China. ✉email: suyunai@bjmu.edu.cn; ljt_102124@163.com; si.tian-mei@163.com

Received: 7 November 2023 Revised: 4 November 2024 Accepted: 13 November 2024
Published online: 22 November 2024

may contribute to the maturation of PVIs during adolescence, one of which is increased glutamatergic inputs to PVIs [26]. Although ES has been reported to impair the structure [27] and function [28] of PNs in the adult mPFC, how ES affects PN activity and their inputs to PVIs in the adolescent mPFC remains unclear.

Current pharmacological (e.g., first-line antidepressants or antipsychotics) and nonpharmacological [e.g., repeated transcranial magnetic stimulation (rTMS)] strategies for the treatment of cognitive impairment have not yielded satisfactory results [5, 29, 30]. Recent clinical and basic studies have highlighted the association between PFC-dependent cognitive dysfunction and corticotropin-releasing hormone (CRH) and its receptor 1 (CRHR1) [31]. Genetic polymorphisms of the CRHR1 gene are associated with cognitive functioning in both healthy adults and patients with psychiatric disorders [32, 33]. In animal studies, down-regulating the CRH-CRHR1 system using pharmacological (e.g., CRH antagonist D-Phe-CRF5; CRHR1 antagonist, antalarmin) or genetic (e.g., prefrontal CRHR1 knockdown) methods could reverse cognitive deficits [27, 34, 35]. However, whether CRHR1-based interventions are effective for treating ES-induced cognitive deficits and how the CRH-CRHR1 system interacts with PFC PVIs in adolescent animals remain unknown. On the other hand, environmental enrichment (EE) nonpharmacological intervention has beneficial effects on stress-related negative outcomes [36], and importantly on ES-induced cognitive impairments in adolescent animals [37, 38]. However, the underlying mechanisms are still unclear.

In this study, we systematically tested the involvement of mPFC PVI activity in ES-induced cognitive deficits in adolescent male mice. We adopted the well-established ES paradigm, the limited nesting and bedding material (LBN), with which we have previously observed deficits in mPFC-dependent cognitive functions and pyramidal neuronal structural plasticity in adult male mice [27]. Here we first evaluated the effects of ES on cognition and mPFC PVI activity in adolescent male mice. We then manipulated mPFC PVI activity through optogenetic and chemogenetic methods to examine the causal link between reduced mPFC PVI activity and ES-induced cognitive deficits. We proposed the following hypothesis to understand the possible causes of reduced PVI activity following ES by, considering (1) the interaction between PVIs and PNs, (2) the involvement of the CRH-CRHR1 system in adverse effects of ES [27, 39–41], and (3) the localization of CRHR1 in PNs [42], by performing genetic manipulation (knockout, overexpression, chemogenetics) to reveal the causal involvement of the PNs and CRHR1 in ES-induced cognitive deficits and reduced PVI activity and to further test whether PVI activity is required in PN and CRHR1 manipulation. Finally, we tested the effects of pharmacological (the CRHR1 antagonist, antalarmin) and nonpharmacological (EE) treatment on cognitive deficits and PVI activity in adolescent male mice.

RESULTS

Early-life stress specifically impaired cognition in adolescent male mice

We first established an LBN model during the postnatal day (PND) 2–9 and then compared a series of stress-related physiological and behavioral measures between stressed and control mice to investigate the effects of early-life stress (ES) on cognition in adolescent male mice (Fig. 1A, B and Fig. S1A). Immediately after stress (PND9), stressed mice exhibited significantly less body weight gain (Fig. S1B, left panel), and the effect persisted into adolescence (Fig. S1B, right panel). Mice exposed to ES also showed significant adrenal atrophy (Fig. S1C) and a tendency for thymic atrophy (Fig. S1D) in adolescence.

Cognitive performance was assessed in four tasks. In the temporal order memory task (TOM, Fig. 1C), stressed mice failed to distinguish the "remote" object from the "recent" object and had a significantly lower discrimination index than control mice. In the Y-maze spontaneous alternation test (Fig. 1D), stressed mice showed lower spontaneous alternation rates and greater error rates for returning to the same arm, indicating spatial working memory deficits. In the novel object recognition test, stressed mice did not distinguish the "novel" object from the "familiar" object as the control mice did (Fig. 1E), despite of no group differences in the discrimination index. Stressed mice also exhibited spatial object recognition deficits, as in this task they failed to discriminate between the "displaced" and "stationary" objects, and showed a significantly lower discrimination index than control mice (Fig. 1F). Motor and exploratory behaviors (i.e., total probe time and distance traveled during the test phase of the recognition tasks or the total arm entries in the Y-maze) were not affected by ES (Fig. S2A–D).

In addition to assessing cognitive behaviors, we also evaluated anxiety-like, social approach, and depression-like behaviors. In the three tasks of anxiety-like behavioral tests, no significant differences were observed between the stressed and control mice (Figs. 1G–I and S2E–G). Social approach was not affected by ES (Figs. 1J and S2H). ES did not significantly affect depression-like behaviors in the tail suspension test (Figs. 1K and S2I), sucrose preference test (Figs. 1M and S2K), or the latency to immobility in the forced swimming test (Fig. S2J), but increased immobility was observed in the stressed mice in the forced swimming test (Fig. 1L).

Together, these behavioral and stress-related physiological results indicate that the adverse effects of ES emerge as early as in adolescent male mice, with cognitive behaviors being particularly vulnerable.

Early-life stress reduced PVI (not SST-IN) activity in the mPFC of adolescent male mice

To examine the involvement of mPFC PVI in the adverse effects of ES during adolescence, we quantified the PVI density and activity in the following three analyses. First, immunohistochemistry revealed that ES significantly decreased the density of PVI in the mPFC, irrespective of the subregion examined (Fig. S3A). The density of somatostatin-expressing interneurons (SST-INs) was not affected (Fig. S3B). Next, using immunostaining for the immediate early gene c-fos (which reflects neural activation [43]) and by performing a colocalization analysis, we found that stressed mice showed a lower density (Fig. 2B) and percentage (Fig. S3C) of PVIs that co-express c-fos in the mPFC, but not in the hippocampus (Fig. S3E–G), during the TOM test. However, no effects of stress were observed on the SST-INs (Figs. 2C and S3D). Finally, we recorded the evoked and spontaneous action potentials in mPFC PVIs in PV-Cre::Ai14 mice through whole-cell voltage clamping to validate the effects of ES on mPFC PVI activity (Fig. 2D). Compared with those of controls, the PVIs of stressed mice showed a significantly lower frequency of evoked action potentials in response to current injection (Fig. 2E) and ES-induced suppression was mainly observed at currents greater than 200 pA. The spontaneous action potentials were not altered by ES (Fig. 2F). Together, these results indicate that ES specifically reduced the PVI density and activity (not SST-INs) in the mPFC of adolescent male mice.

How does ES reduce PVI activity in the mPFC? The functional maturation of PVIs in the adolescent mPFC involves several mechanisms [21, 26], such as increased glutamatergic inputs and an increased density of perineuronal net (PNN) proteins. As PNs form robust functional synapses on PVIs, reduced PVI activity may result from reduced excitatory inputs to PVIs. We thus examined the effects of ES on excitatory inputs from PNs to PVIs, using optogenetics and electrophysiological recordings (Fig. 2G, H). We first confirmed the presence of monosynaptic connections between PNs and PVIs (Fig. S3H). We then compared the optically-evoked excitatory postsynaptic current (oEPSC) in mPFC

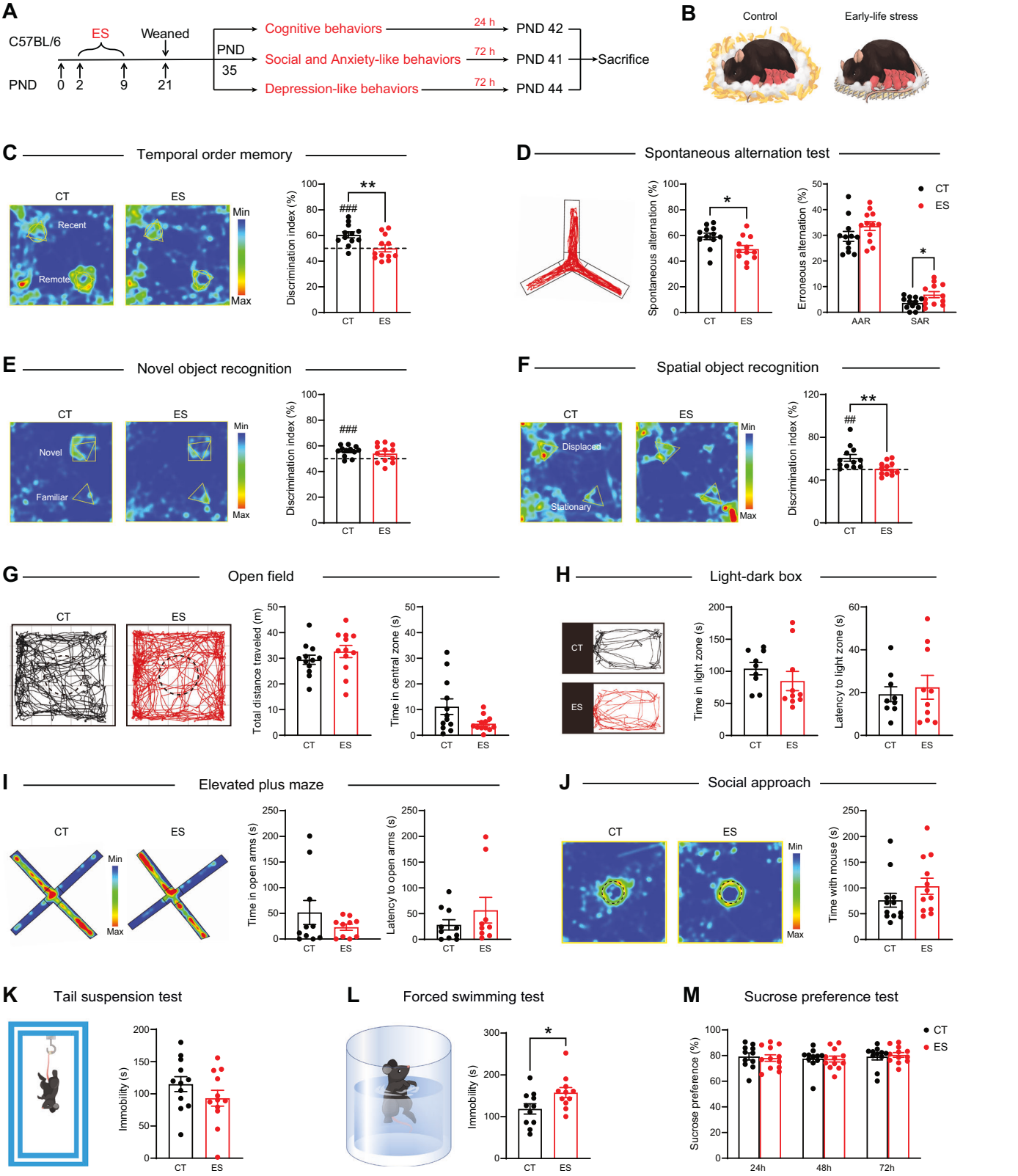

PVIs in two groups of PV-Cre mice after PN activation. The results showed that ES significantly reduced the oEPSC frequency but not the oEPSC amplitude (Fig. 2I), and increased paired-pulse ratio (PPR) value (Fig. 2J), suggesting that ES indeed reduced the excitatory inputs on PVIs following PN activation. Converging evidence was obtained when we quantified the expression levels of vesicular glutamate transporter-1 (VGluT1, responsible for loading glutamate into synaptic vesicles for future release [44] and involved in the regulation of excitatory neurotransmission [45]) at different distances from the soma of PVIs (Fig. S4A–D). No

Fig. 1 Early-life stress specifically impaired cognition in adolescent male mice. A Experimental timeline of ES, behavioral tests, and brain tissue acquisition. **B** A schematic illustration of control (left panel) and ES (right panel) housing conditions. While the control mice lived in cages with sufficient bedding/nesting conditions, the ES dam and pups lived in cages with limited nesting and bedding materials. **C**–**F** Cognitive behavioral tests and results. The left panels in (**C**, **E**, and **F**) are representative maps showing the time spent in each location by CT and ES mice; warm colors represent more time. **C** Temporal order memory test. Right panel, the percentage of time spent probing the "remote" and "recent" object (one sample *t*-test between two objects: CT: $t_{11} = 4.475$, $p = 0.001$; ES: $t_{11} = 0.006$, $p = 0.996$; unpaired *t*-test: $t_{22} = 2.911$, $p = 0.008$). **D** Y-maze spontaneous alternations. Left panel, representative motion path in the test; middle, spontaneous alternation ratio ($t_{22} = 2.676$, $p = 0.014$, unpaired *t*-test). Right panel, erroneous alternations: alternative arm return (AAR: $t_{22} = 1.549$, $p = 0.136$, unpaired *t*-test) and same arm return (SAR: $t_{22} = 2.381$, $p = 0.026$, unpaired *t*-test). **E** Novel object recognition test. Right panel, the percentage of time spent probing the "novel" object and "familiar" object (one sample *t*-test between two objects: CT: $t_{11} = 4.839$, $p = 0.001$; ES: $t_{11} = 2.003$, $p = 0.0704$; unpaired *t*-test: $t_{22} = 0.806$, $p = 0.008$). **F** Spatial object recognition test. Right panel, the percentage of time spent probing the "displaced" and "stationary" object (one sample *t*-test: CT: $t_{11} = 3.426$, $p = 0.006$; ES: $t_{11} = 0.358$, $p = 0.727$; unpaired *t*-test: $t_{22} = 2.819$, $p = 0.010$). **G**–**I** Anxiety-like behavioral tests and results. **G** Open field test. Left panel, representative motion paths of CT and ES mice. Middle panel, total distance traveled in 10 min ($t_{22} = 1.073$, $p = 0.295$, unpaired *t*-test). Right panel, time spent in center zone ($t_{12.73} = 2.095$, $p = 0.057$, unpaired *t*-test with Welch's correction). **H** Light–dark box test. Left panel, representative motion paths in the light chamber for CT and ES mice. Middle panel, time in the light chamber ($t_{17} = 1.051$, $p = 0.308$, unpaired *t*-test). Right panel, latency to reach the light chamber ($t_{17} = 0.482$, $p = 0.636$, unpaired *t*-test). **I** Elevated plus maze test. Left panel, representative map showing the time spent in each location by CT and ES mice; warm colors represent more time. Middle panel, time spent in the open arms ($t_{10.17} = 1.184$, $p = 0.263$, unpaired *t*-test with Welch's correction). Right panel, latency to open arms ($t_{10.52} = 1.053$, $p = 0.316$, unpaired *t*-test with Welch's correction). **J** Social approach test. Left panel, representative map showing the time spent in each location by CT and ES mice; warm colors represent more time. Right panel, time spent interacting with stranger mice ($t_{22} = 1.320$, $p = 0.201$, unpaired *t*-test). **K**–**M** Depressive-like behavioral tests and results. **K** Tail suspension test. Left panel, diagram of the test. Right, immobility time within 6 min ($t_{22} = 2.095$, $p = 1.299$, unpaired *t*-test). **L** Forced swimming test. Left panel, diagram of the test; Right panel, immobility time within 6 min ($t_{20} = 2.260$, $p = 0.035$, unpaired *t*-test). **M** Sucrose preference test. The percentage of sucrose preference (stress effect, $F_{(1,\ 63)} = 0.001$, $p = 0.976$; time effect, $F_{(2,\ 63)} = 0.493$, $p = 0.613$; stress × time interaction, $F_{(2,\ 63)} = 0.148$, $p = 0.863$). Data are represented as mean ± SEM. $^{*}p < 0.05$ and $^{**}p < 0.01$ for comparisons between the CT and ES group; $^{\#\#}p < 0.01$ and $^{\#\#\#}p < 0.001$, one sample *t*-test. AAR alternative arm return, CT control, ES early-life stress, PND postnatal day, SAR same arm return. See also Figs. S1–S2.

significant group differences were detected for PNNs (Fig. S4E–G), a component of the extracellular matrix that preferentially surrounds PVIs and modulates their excitability [46]. These results indicate that the ES-induced reduction in PVI activity may result from reduced excitatory inputs from PNs in the mPFC.

Prefrontal PVI activity mediates early-life stress-induced cognitive deficits in adolescent mice

Having shown that ES elicited both cognitive deficits and reduced mPFC PVI activity in adolescent mice, in this section we examined whether the reduced mPFC PVI activity causally mediates ES-induced cognitive deficits in adolescent mice using chemogenetic and optogenetic techniques. First, we performed the experiments described below to mimic the ES-induced reduction in the PVI density and activity in the mPFC and to evaluate the corresponding behavioral consequences.

First, a loss-of-function experiment was performed to selectively ablate mPFC PVIs in PV-Cre mice by injecting an adeno-associated virus (AAV) expressing Cre-dependent Casp3 (a cell apoptosis effector molecule) into the mPFC at PND22 (Fig. S5A, B). This manipulation resulted in cognitive deficits, including lower discrimination indices in the TOM test (Fig. S5C) and in the novel object recognition test (Fig. S5E), and higher error rates for same arm return (SAR) in the Y-maze spontaneous alternation test (Fig. S5D). The performance on the spatial object recognition task was not affected by mPFC PVI ablation (Fig. S5F). Anxiety-like behaviors in the three tasks were also largely unaffected (Fig. S5G–I), except for a reduced time spent in the light box in the light–dark box test (Fig. S5H).

Second, we inhibited mPFC PVI activity via chemogenetic manipulation of DREADDs, i.e., by bilateral injection of an AAV vector carrying Cre-dependent hM4Di (Gi) into the mPFC of PV-Cre mice (Figs. 3A, B and S6A). Immunofluorescence staining combined with colocalization verified that the CNO group showed significantly lower density (Fig. 3C) and percentage (Fig. S6B) of virus-infected PVIs that co-expressed c-fos, than did the Veh group, indicating that PVI activity was inhibited. This manipulation again resulted in cognitive deficits in the TOM and Y-maze spontaneous alternation tests. In the TOM task (Fig. 3D), mice in the CNO group showed a lower reduced discrimination index than those in the Veh group and they were unable to discriminate between the "remote" and "recent" objects. In the Y-maze spontaneous alternation test (Fig. 3E), CNO-treated mice showed higher error rates for SAR; no group differences were observed in the SA or AAR test. The performance on the novel object recognition (Fig. S6C) and spatial object recognition (Fig. S6D) tasks was not significantly affected by CNO treatment. CNO treatment did not affect anxiety-like behaviors in the open field test (Fig. S6E, F), but reduced amount of the time spent in the light box in the amount of light–dark box test (Fig. S6G) and the time spent in the open arms in the elevated plus maze (Fig. S6H), indicating of increased anxiety levels following PVI inhibition in mPFC, which is consistent with previous findings [16].

Optogenetic manipulation was then performed to validate the above-mentioned chemogenetic results (Figs. 3F–I and S7A, B). As the previous two experiments support the consistent involvement of mPFC PVIs in the performance of animals on the TOM and Y-maze spontaneous alternation tests, these two behavioral tests were conducted in the subsequent experiments. Optogenetic inhibition of mPFC PVIs disrupted temporal order memory and spatial working memory. In the TOM task (Fig. 3H), eNpHR3.0-infected mice failed to discriminate between the "remote" and "recent" objects and exhibited a lower discrimination index than control mice. In the Y-maze spontaneous alternation test (Fig. 3I), eNpHR3.0-infected mice displayed more errors of alternate arm return than EGFP-infected mice; no group differences were found for SA or SAR.

Finally, based on the three experiments above showing that PVI inhibition reproduced ES-induced impairments in PFC-dependent cognitive functions, we continued to investigate whether upregulating mPFC PVI activity could reverse the cognition-impairing effects of ES by bilaterally injecting an AAV vector carrying Cre-dependent hM3Dq (Gq) into the mPFC in PV-Cre mice (Figs. 3J, K and S8A). The efficiency and specificity of the DREADD system were tested by detecting, c-fos immunoreactivity was detected in mCherry-infected neurons and PVIs after a single CNO injection. The density and percentage of mCherry-infected neurons co-labeled with c-fos were significantly elevated by DREADDs (Fig. S8B, C). For the immunofluorescence staining for c-fos and PV colabeling, two-way ANOVA revealed the main

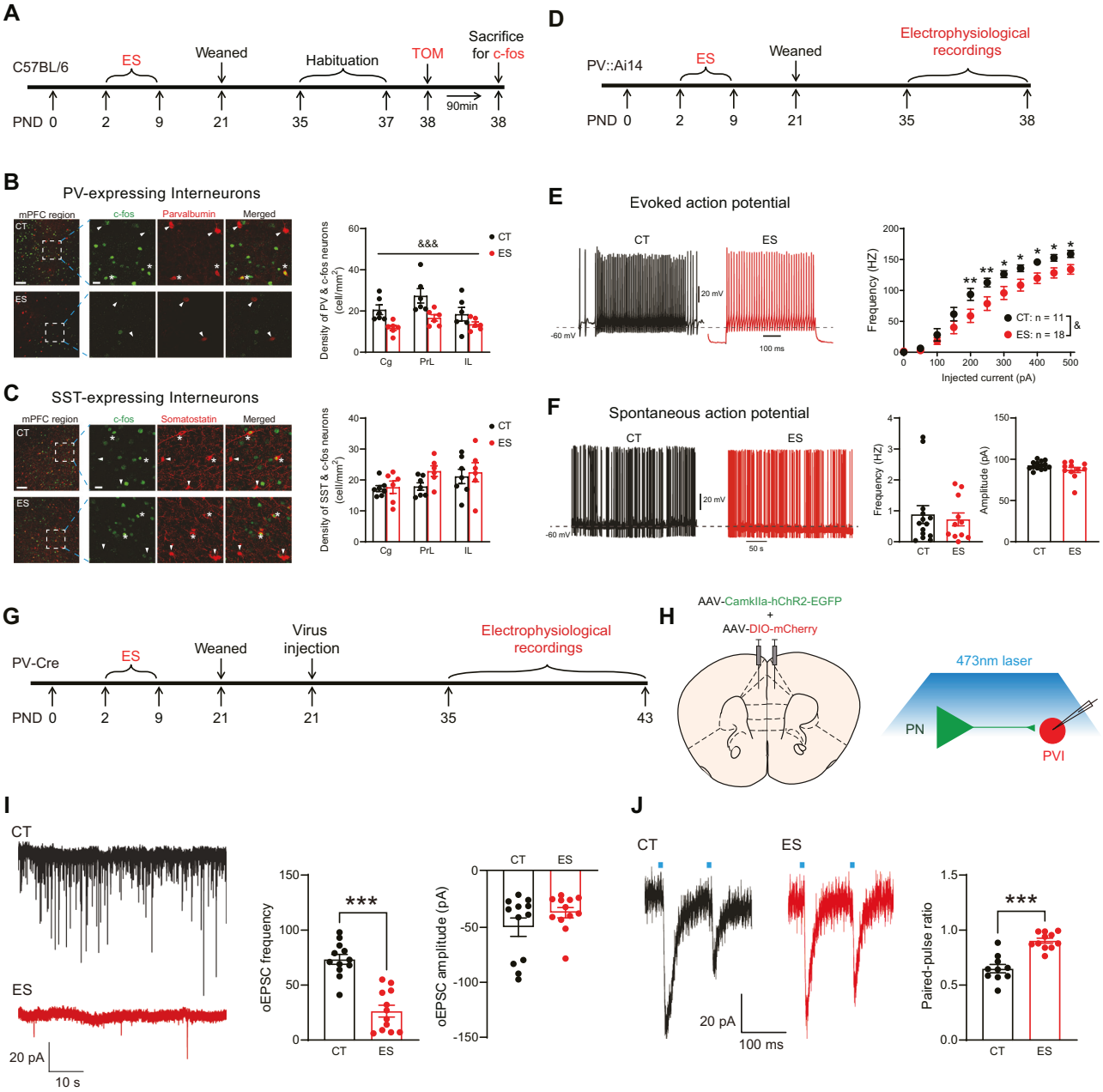

effects of CNO for PVI density (Fig. 3L) and a significant stress × drug interaction for PVI percentage (Fig. S8D). Further group comparisons revealed that c-fos expression in PVIs was decreased by ES, which was reversed by DREADDs (Fig. S8D). In terms of behavioral consequences, two-way ANOVA revealed a significant stress × drug interaction for the TOM task (Fig. 3M). Selective activation of mPFC PVIs restored the ES-induced impairment. No effects of stress or CNO were observed on the total probe time or total distances traveled in the test phase (Fig. S8E). For the Y-maze spontaneous alternation task (Figs. 3N and Fig. S8F), two-way ANOVA revealed significant stress × CNO interactions for SA and SAR. The negative stress effects induced by ES were attenuated by the activation of mPFC PVIs. These results indicate that increased mPFC PVI activity is sufficient to alleviate ES-induced cognitive deficits in temporal order memory and spatial working memory.

By selectively downregulating and upregulating mPFC PVI activity, the four experiments described above provide causal evidence that mPFC PVI activity mediates ES-induced cognitive deficits in adolescent male mice.

Prefrontal pyramidal neurons are involved in early-life stress-induced cognitive deficits through PVIs

Based on our observation that ES reduced the excitatory inputs from local PNs to PVIs (Fig. 2I, J), we examined whether the reduced excitatory inputs may result from reduced PN activity. We measured mPFC PN activity during the TOM test using immunofluorescence staining combined with the colocalization of c-fos and neurogranin or CamkIIa (two excitatory neuron markers [47, 48]). Compared with control mice, stressed mice showed reduced density and percentage of neurons with the colabeling for c-fos and neurogranin (Figs. 4A and S9A) or CamkIIa (Fig. S9B–D), indicative of ES-induced inhibition of PN activity during the TOM test. Reduced PN activity was confirmed by electrophysiological recordings: ES significantly decreased the frequency of evoked action potentials in mPFC PN activity, especially at currents greater than 400 pA (Fig. 4B). The

Fig. 2 Early-life stress reduced PVIs (not SST-INs) activity in the mPFC of adolescent male mice. A–C Quantification of the density of PVIs or SST-INs that were c-fos-positive in CT and ES mice during the TOM test. **A** Experimental timeline of ES exposure, behavioral tests, and brain tissue acquisition from C57BL/6 mice. **B** Top panel, representative images showing the co-expression of c-fos and PV in the mPFC of CT and ES mice. Asterisks indicate neurons that co-express c-fos and PV; arrowheads indicate PV-expressing cells without detectable c-fos expression. Scale bar, 100 μm or 20 μm. Bottom panel: the density of neurons showing PV and c-fos colocalization in the three subfields of mPFC in two groups (Stress effect, $F_{(1, 24)} = 17.78$, $p < 0.001$). **C** Top panel, representative images show the co-expression of c-fos and SST in the mPFC of CT and ES mice. Asterisks indicate neurons that co-express c-fos and SST; arrowheads indicate SST-expressing cells without detectable c-fos expression. Scale bar, 100 μm or 20 μm. Bottom panel: the density of neurons showing SST and c-fos colocalization in the three subfields of the mPFC in the two groups (Stress effect, $F_{(1, 24)} = 1.969$, $p = 0.170$). **D–F** Effects of ES on the intrinsic excitability of PVIs in the mPFC. **D** The experimental timeline of electrophysiological recordings in the mPFC in adolescent male PV::Ai14 mice. **E** Evoked action potentials. Left panel, sample traces in response to a 500-pA current step of CT and ES mice. Right panel, ES reduced the frequency of evoked action potentials in response to the current injection (≥200 μA, all $p < 0.044$, unpaired *t*-test). **F** Spontaneous action potentials. Left panel, sample traces of spontaneous potential in CT and ES mice. Right panel, ES did not alter the frequency and amplitude of the spontaneous action potential of PVIs. **G–J** Effects of ES on the excitatory transmission of PNs to PVIs. **G** The experimental timeline of electrophysiological recordings in the mPFC of adolescent male PV-Cre mice. **H** Schematic of virus injection and the recording strategy in PVIs in acute slice. **I, J** oEPSCs in PVIs in response to optical stimulation (473 nm, 10-ms pulse width at 100-ms interval) on PNs in the mPFC. **I** The frequency and amplitude of oEPSCs. Left panel, representative traces of oEPSC of CT and ES groups. Right panel, quantification of oEPSC frequency ($t_{22} = 6.723$, $p < 0.001$, unpaired *t*-test) and amplitude ($t_{22} = 1.373$, $p = 0.184$, unpaired *t*-test with Welch's correction) of PVIs. **J** PPR of oEPSCs. Left panel, representative traces of PPR of CT and ES groups. Right panel, quantification of PPR ($t_{19} = 5.908$, $p < 0.001$, unpaired *t*-test). Data are represented as mean ± SEM. $^{*}p < 0.05$, $^{**}p < 0.01$ and $^{***}p < 0.001$, comparisons between CT and ES group; $^{\&}p < 0.05$ and $^{\&\&\&}p < 0.001$ for the effect of stress in the two-way ANOVA. Cg cingulate cortex, CT control, ES early-life stress, IL infralimbic cortex, mPFC medial prefrontal cortex, oEPSC optical-evoked excitatory postsynaptic current, PN pyramidal neuron, PND postnatal day, PPR paired-pulse ratio, PrL prelimbic cortex, PVI parvalbumin-expressing interneuron, SST-IN somatostatin-expressing interneuron, TOM temporal order memory. See also Figs. S3–S4.

spontaneous action potentials were not affected (Fig. S9E). We performed chemogenetic experiments to examine the causal involvement of PNs in the adverse effects of ES on adolescent mice.

First, we tested whether inhibiting PN activity in adolescent mice could reproduce the cognitive deficits caused by ES (Fig. S10A–F). Specifically, we bilaterally injected an AAV vector expressing Cre-dependent hM4Di (Gi) into the mPFC of CamkIIa-Cre mice. Dual immunofluorescence staining for mCherry^{+} and c-fos^{+} (Fig. S10B) showed that, compared with those in the Veh group, the percentage of neurons co-expressing mCherry^{+} and c-fos^{+} in the CNO group was decreased. In terms of cognitive performance, in the TOM task, CNO-treated mice failed to discriminate between the "remote" and "recent" objects and exhibited a lower discrimination index (Fig. S10C). In the Y-maze test, CNO-treated mice showed lower SA and higher error rates of alternate arm return compared with Veh-treated mice (Fig. S10E). No significant group differences were observed in motor or exploratory behaviors in the two tasks (Fig. S10D, F). Namely, selective inhibition of mPFC PNs reproduces ES-induced deficits in temporal order memory and spatial working memory.

Second, we investigated whether activating PNs (Fig. 4C) could reverse the ES-induced cognitive impairment. Chemogenetic activation of mPFC PNs in C57 mice was found to increase the density and percentage of PVIs that co-express c-fos in mPFC during the TOM test (Fig. S11), indicating that local PNs are a significant regulator of mPFC PVIs. Then, for the cognitive tests, with selective activation of PNs in vivo (Figs. 4D–F and S12A), we observed a significant stress × CNO interaction (Fig. 4G) in the TOM task in that PN activation restored the decreased discrimination index in ES-treated mice. For the Y-maze spontaneous alternation task (Fig. 4H), two-way ANOVA revealed significant effects of stress × drug interactions on SA and SAR. The negative effects of stress on these measures were attenuated by the activation of the prefrontal PNs. No effects of stress or CNO were observed on motor or exploratory behaviors in the two tasks (Fig. S11B, C). Thus, the selective activation of mPFC PNs reverses ES-induced deficits in temporal order memory and spatial working memory.

Based on the above-mentioned results showing that ES reduced the functional activity of PNs and PVIs and the excitatory inputs between them, we hypothesized that the cognition-improving effects of PN activation may be mediated by the PVIs. To test this hypothesis, we conducted a double chemogenetic manipulation experiment to activate PNs and inhibit PVIs in the mPFC and examined whether PVI inhibition could block the effect of PN activation on reversing ES-induced cognitive deficits. Double chemogenetic manipulation was achieved by bilateral injection of a mixture of two viruses (AAV-CamkIIa-Gq; Cre-dependent AAV-DIO-Gi) into the mPFC of adolescent PV-Cre mice (Fig. 4I). Immunofluorescence staining for mCherry, PV, and c-fos was performed to examine the c-fos-positive neurons that were mCherry^{+} (non-PV^{+}) or PV^{+} for validation. For mCherry^{+} (non-PV^{+}) and c-fos^{+} neurons (Figs. 4J and S13A), we observed both the main effect of CNO and the effect of stress × CNO interaction. *Post hoc* tests with Bonferroni's correction showed that PNs were activated in both control and stressed mice. For PV^{+} and c-fos^{+} neurons (Figs. 4K and S13B), we also observed both a main effect of CNO and an effect of the stress × CNO interaction. Namely, PVI activity was inhibited in control mice after CNO administration and was reduced in ES-exposed vehicle-treated mice; CNO did not further decrease PVI activity in stressed mice. For cognitive effects, in the TOM task (Fig. 4L), two-way ANOVA revealed a tendency toward a main effect of CNO and an effect of the stress × CNO interaction. Therefore, selective inhibition of mPFC PVIs blocked the effect of PNs activation on reversing the TOM impairment induced by ES. In addition, the double chemogenetic manipulation significantly reduced the discrimination index in control mice, which resembled previous results of PVI inhibition. For the Y-maze test (Fig. 4M), two-way ANOVA revealed a significant main effect of stress on SA, indicating the absence of reversal effects of PN activation after PVI inhibition. The main effects of CNO were also observed for AAR and SAR, as CNO significantly increased AAR and decreased SAR. No effects of stress or CNO were observed on motor or exploratory behaviors in the two tasks (Fig. S13C, D). Together, these results indicate that inhibition of PVIs in the mPFC could block the effect of PN activation on reversing ES-induced cognitive deficits, supporting the indispensable role of PVIs in the cognition-improving effects of PNs.

Finally, we performed another double chemogenetic manipulation experiment, in which we inhibited PNs and activated PVIs in the mPFC in adolescent mice exposed to ES to verify whether PVI activation would still reverse ES-induced cognitive deficits when PNs were inhibited (Fig. S14A). The results showed that the activation of PVIs could still significantly ameliorate ES-induced cognitive deficits in temporal order memory (Fig. S14B, C) and spatial working memory (Fig. S14D, E), supporting the powerful influence of mPFC PVIs on the ES-induced cognitive impairment in adolescent male mice, regardless of PNs.

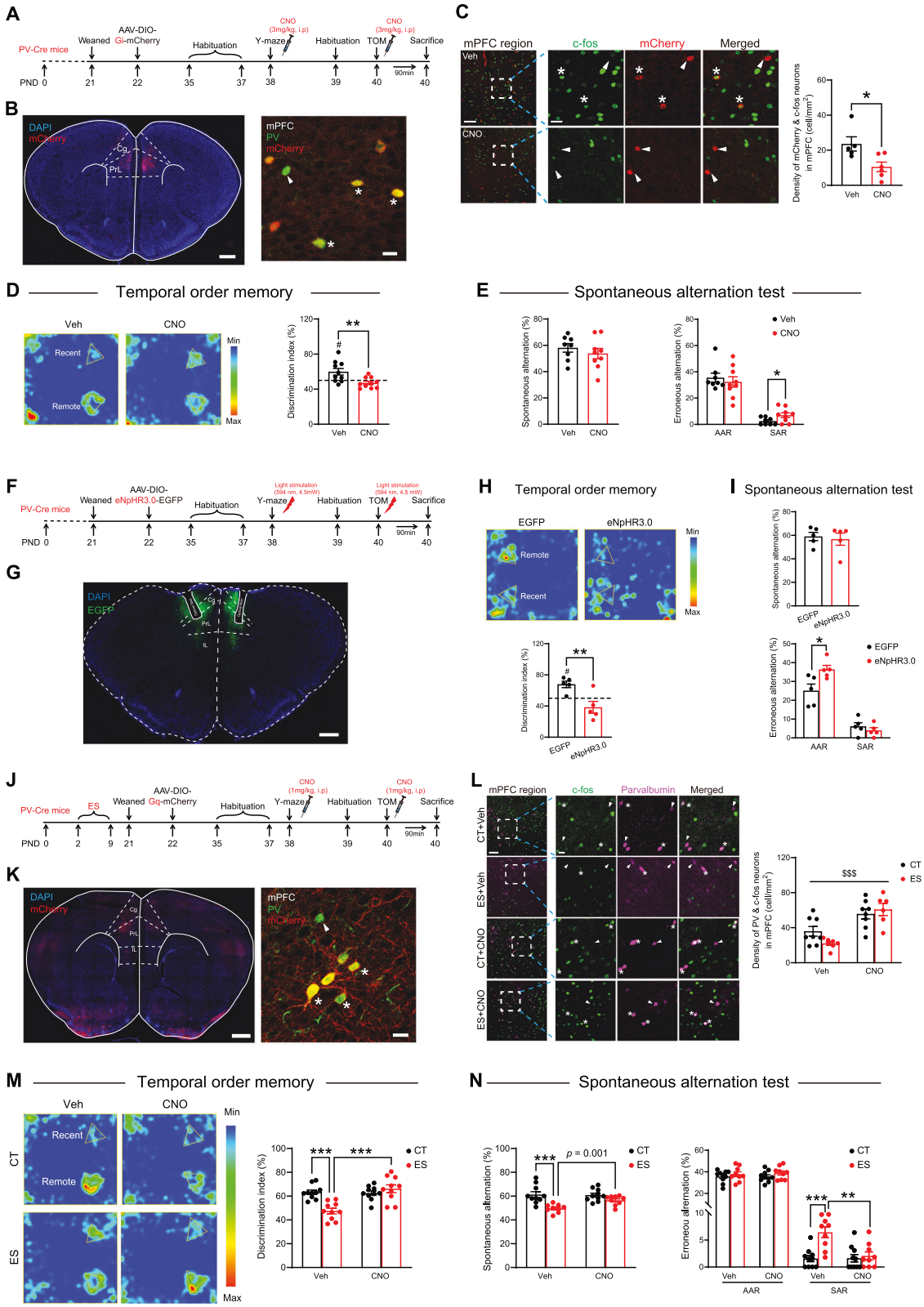

CRHR1 downregulation reverses early-life stress-induced cognitive deficits in adolescent mice by restoring PVI activity in the mPFC

We have previously established the involvement of the CRH-CRHR1 system in ES-induced behavioral and neural abnormalities [27, 39–41, 49] in postnatal and adult mice. Here we extended this line of research to adolescent mice and tested how the CRH-CRHR1 system interacts with PNs or PVIs. As CRHR1 is mainly expressed in PNs in the cortex [42], we first confirmed that *Crhr1* mRNA is indeed primarily expressed in pyramidal, not inhibitory, neurons, in the mPFC (Fig. 5A) by quantifying the colocalization of *Crhr1* mRNA with *Slc17a7* (the mRNA encoding VGluT1, an

Fig. 3 Prefrontal PVI activity mediates early-life stress-induced cognitive deficits in adolescent male mice. A–E Chemogenetic inhibition of mPFC PVI activity impairs cognition. **A** Experimental timeline of the behavioral tests, CNO injection, and brain tissue acquisition after hM4D(Gi) virus injection in adolescent PV-Cre mice. **B** Left panel, representative image showing region-specific expression of mCherry in the mPFC; right panel, representative image showing that the majority of PVIs express hM4Di in the mPFC. Asterisks indicate neurons that co-express mCherry and PV; arrowheads indicate PV-expressing cells without detectable mCherry expression. Scale bar, 500 μm or 20 μm. **C** Representative images show the expression of c-fos and mCherry in the mPFC of Veh and CNO mice. Asterisks indicate neurons that co-express mCherry and c-fos, while arrowheads indicate mCherry-expressing cells without detectable c-fos expression. Scale bar, 100 μm or 20 μm. Immunostaining analyses confirmed that Gi decreased in the expression of c-fos in PVIs in the mPFC ($t_9 = 2.748$, $p = 0.023$, unpaired *t*-test). Chemogenetic inhibition of mPFC PVI activity impaired (**D**) temporal order memory (Paired *t*-test: Veh: $t_9 = 2.617$, $p = 0.028$; CNO: $t_9 = 1.495$, $p = 0.169$; unpaired *t*-test: $t_{18} = 3.010$, $p = 0.008$) and **E** spatial working memory in the Y-maze spontaneous alternation test (SAR: $t_{15} = 2.135$, $p = 0.050$, unpaired *t*-test) in adolescent mice. **F–I** Optogenetic inhibition of mPFC PVI activity impairs cognition. **F** Experimental timeline of the behavioral tests, light stimulation, and brain tissue acquisition after eNpHR3.0 viral infection in adolescent PV-Cre mice. The light stimulation protocol was 594 nm laser, 4–5 mW, OFF-ON-OFF-ON, 2 min/section. **G** Representative image showing the location of bilateral viral infection and optic-fiber implantation in mPFC. Scale bar, 500 μm. Optogenetic inhibition of mPFC PVI activity impaired (**H**) temporal order memory (Paired *t*-test: EGFP: $t_4 = 4.301$, $p = 0.013$; eNpHR3.0: $t_4 = 1.542$, $p = 0.198$; unpaired *t*-test: $t_8 = 3.414$, $p = 0.009$) and (**I**) increased AAR in the Y-maze spontaneous alternation test ($t_8 = 2.709$, $p = 0.027$, unpaired *t*-test) in adolescent mice. **J–N** Chemogenetic activation of mPFC PVI activity reverses ES-induced cognitive deficits. **J** The experimental timeline of the behavioral tests, CNO injection, and brain tissue acquisition after hM3D(Gq) virus injection in adolescent PV-Cre mice. **K** Left panel, representative image showing region-specific expression of mCherry in the mPFC; right panel, representative image showing that the majority of PVIs express hM3Dq in the mPFC. Asterisks indicate neurons that co-express mCherry and PV; arrowheads indicate PV-expressing cells without detectable mCherry expression. Scale bar, 500 μm or 20 μm. **L** Representative images showing the expression of c-fos and PV in the mPFC of the four groups of mice. Immunostaining analyses reveal that the number of activated PVI neurons in the mPFC in the temporal order memory test was increased by CNO injection (CNO effect: $F_{1, 25} = 30.32$, $p < 0.001$; two-way ANOVA). Asterisks indicate neurons that co-express PV and c-fos; arrowheads indicate PV-expressing cells without detectable c-fos expression. Scale bar, 100 μm or 20 μm. **M**, **N** Activation of PVIs in the mPFC reverses the ES-induced deficits of temporal order memory (**M**, CT-Veh *vs*. ES-Veh: $p < 0.001$, ES-Veh *vs*. ES-CNO: $p < 0.001$, Bonferroni's test) and spatial working memory (**N**, SA: CT-Veh *vs*. ES-Veh: $p < 0.001$, Bonferroni's test; ES-Veh *vs*. ES-CNO: $p = 0.001$, unpaired *t*-test; SAR: CT-Veh *vs*. ES-Veh: $p < 0.001$, ES-Veh *vs*. ES-CNO: $p = 0.002$, Bonferroni's test). Data are represented as mean ± SEM. $^{*}p < 0.05$, $^{**}p < 0.01$ and $^{***}p < 0.001$, unpaired *t*-test or Bonferroni's *post hoc* test; $^{\#}p < 0.05$, one sample *t*-test. AAR alternative arm return, CNO clozapine-N-oxide, CT control, ES early-life stress, mPFC medial prefrontal cortex, PND postnatal day, PVI parvalbumin-expressing interneuron, SA spontaneous alternation, SAR same arm return, Veh vehicle. See also Figs. S5–S8.

excitatory neuron marker) and *Slc32a1* (the mRNA encoding the GABA vesicular transporter, an inhibitory neuron marker) using single-molecule fluorescence in situ hybridization (RNAscope ISH). We then used RT-qPCR to directly test whether ES altered the expression of the *Crh* and *Crhr1* mRNAs in the mPFC of adolescent male mice. The results showed that ES significantly increased the expression of the *Crhr1* mRNA (Fig. 5B) but not the *Crh* mRNA (Fig. S15). Together with previous reports that ES increased the number of CRH-immunoreactive cells in the adult hippocampus [50] and that the administration of CRHR1 antagonists (e.g., antalarmin) could reverse the negative effects of ES [27, 49], these results consistently show that ES leads to the upregulation of the CRH-CRHR1 system in mice.

We overexpressed CRH in CRH-positive neurons of the mPFC and investigated the effects of CRHR1 activation on the functional activity of PNs, PVIs, and cognitive behaviors in adolescent male mice to provide direct evidence that CRHR1 activation causes decreased activity in mPFC PNs and subsequent effects (Fig. S16A). We bilaterally injected a mixture of CRH-Cre and AAV vectors carrying the *Crh* gene into the mouse mPFC at PND22 (Fig. S16B). CRH overexpression in the mPFC was confirmed by western blot analyses (Fig. S16C). Fluorescence staining revealed that CRH overexpression decreased the percentage and density of PNs (Fig. S16D) and PVIs (Fig. S16E) expressing c-fos in the mPFC. Temporal order memory (Fig. S16F, G) and spatial working memory (Fig. S16H, I) in adolescent male mice were also significantly impaired by CRH overexpression. This gain-of-function experiment suggested that CRHR1 activation by CRH from mPFC CRH-positive neurons mimics the detrimental effects of ES on PN/PVI activity and cognition.

We then investigated whether blocking the mPFC CRH-CRHR1 system could reverse ES-induced deficits in PVIs and temporal order memory. We constructed an AAV vector carrying sgRNA targeting *Crhr1* to achieve CRISPR-Cas9-mediated deletion of CRHR1 (Fig. 5C). Five gRNAs were screened using in vitro cellular assays and the sgRNA3 sequence with the most effective transfection was chosen for packaging (Fig. S17A). Staining for the HA tag confirmed that the virus was mainly present in the mPFC (Fig. S17B). For the TOM task, significant reversal effects were observed: CRHR1 deletion restored the temporal order memory impairment induced by ES (Figs. 5D and S17C). Two-way ANOVA revealed a significant effect of the stress × virus interaction on PVI activity in the mPFC (Figs. 5E, F, and S17D): CRHR1 deletion reversed the ES-induced reduction in PVI activity. Furthermore, the discrimination index in the TOM task significantly correlated with PVI activity in the mPFC across all the animals (Fig. 5G). Together, these results suggest that ES may first upregulate CRHR1 in prefrontal PNs, which reduces the activity of local PNs and their excitatory inputs to PVIs, and in turn, downregulates PVI activity and leads to cognitive impairments.

Motivated by the recently established association between the CRH-CRHR1 system and cognition in the literature [31], we next performed two pharmacological intervention experiments using the CRHR1 antagonist antalarmin. In the first experiment, antalarmin was intraperitoneally injected daily during stress procedure (PND2-8, Fig. 5H). The TOM task and PVI activity were then assessed in adolescent mice. For TOM, two-way ANOVA revealed a significant effect of the stress × drug interaction, as antalarmin reversed the ES-induced reduction in the discrimination index (Fig. 5I). No significant group differences were observed in motor or exploratory behaviors in the test stage (Fig. S17E). Regarding PVI activity in the mPFC, immunofluorescence staining for c-fos and PV showed significant main effects of stress and antalarmin, without a stress × drug interaction (Figs. 5J, K and S17F). Namely, the density and percentage of PVIs co-labeled with c-fos were significantly reduced by ES and increased by antalarmin. Similar effects of ES and antalarmin on the density of neurogranin^{+} neurons co-labeled with c-fos were observed (Fig. S17G, H). Furthermore, the discrimination index in the TOM task significantly correlated with PVI (Fig. 5L) and PN (Fig. S17I) activity in the mPFC. In the second experiment, the drug was administered to adolescent stressed and control mice 30 min prior to the TOM test to examine the acute pharmacological effects of antalarmin (Fig. 5M). Similar stress × drug interactions were observed for TOM and mPFC PVIs. The acute antalarmin injection blocked the ES-induced reductions in the discrimination index (Figs. 5N and S17I) and the mPFC PVIs activity

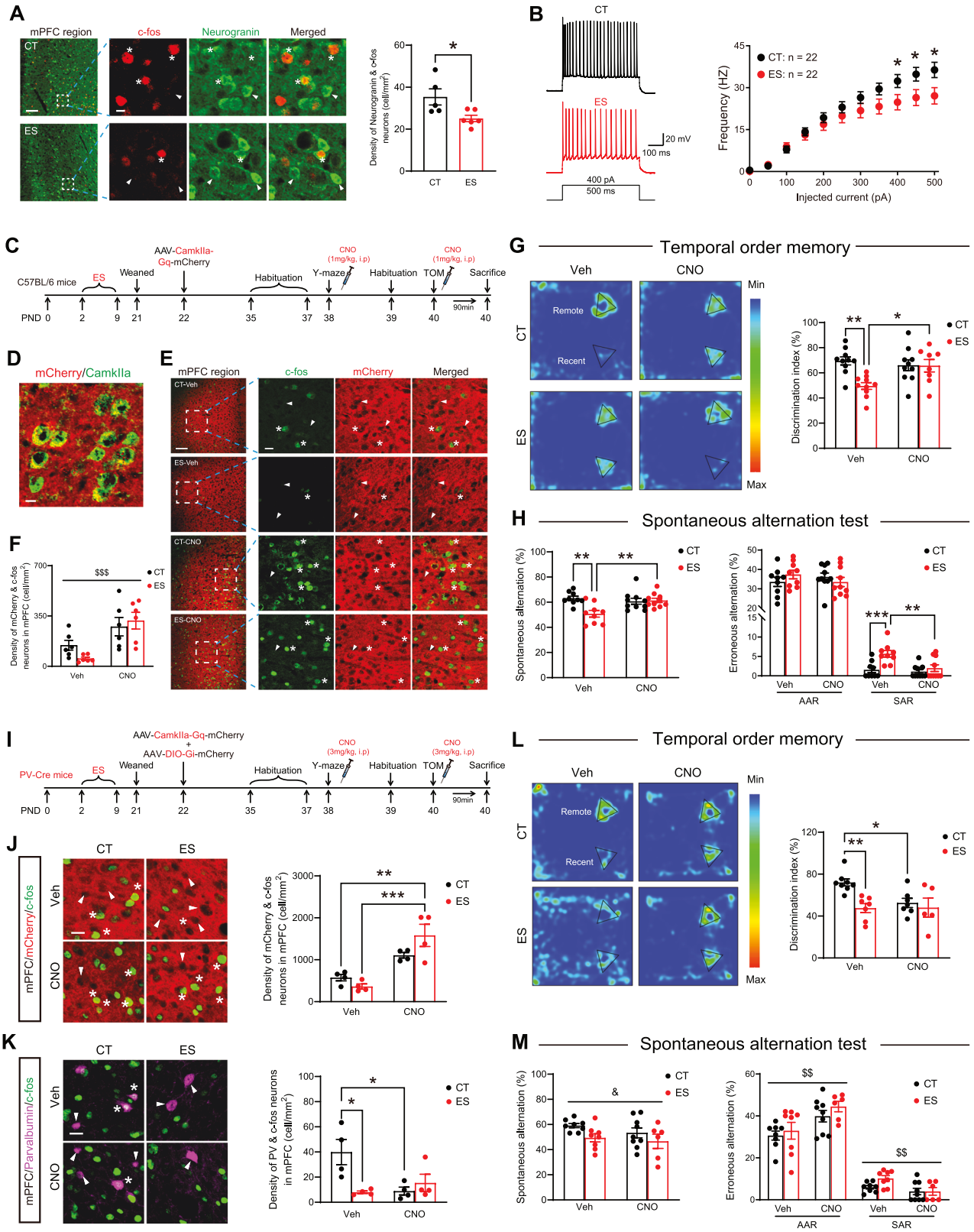

(Figs. 5O, P and S17J). A significant correlation between the discrimination index and PVI activity in the mPFC was observed (Fig. 5Q).

We conducted an experiment to examine the effects of PVI inhibition on the therapeutic efficacy of acute antalarmin treatment to test the hypothesis that the cognition-improving effects of antalarmin may be mediated by PVI activity in the mPFC (Fig. 5R, S). For the assessment of PVI activity in the mPFC of stressed mice receiving antalarmin treatment, immunofluorescence staining for c-fos and PV showed that the density (Fig. 5T)

Fig. 4 Prefrontal PN activity mediates early-life stress-induced cognitive deficits by enhancing PVI activity in adolescent male mice. A The effects of ES on the mPFC PN activity. The left panels in (**A**) depict representative images showing the co-expression of c-fos and or Neurogranin in the mPFC of CT and ES mice. Asterisks indicate co-expressing neurons; arrowheads indicate neurogranin-expressing cells without detectable c-fos expression. Scale bar, 100 μm or 10 μm. Right panels show that ES reduces the density of c-fos- and neurogranin-co-expressing neurons ($t_9 = 2.668$, $p = 0.026$, unpaired *t*-test) in the mPFC of adolescent mice during the TOM test. **B** The effects of ES on evoked action potential of PNs. Left panel, sample traces in response to a 500-pA current step of CT and ES mice. Bottom panel, ES reduced the frequency of evoked action potential in response to the current injection (≥400 μA, all $p < 0.043$, unpaired *t*-test). **C**–**H** Chemogenetic activation of mPFC PN activity reverses ES-induced cognitive deficits. **C** Experimental timeline of the behavioral tests, CNO injection, and brain tissue acquisition after CamkIIa-hM3D(Gq) virus injection in adolescent C57BL/6 mice. **D** Representative image showing the co-expression of mCherry and CamkIIa in the mPFC. Scale bar, 10 μm. **E** Representative images showing the expression of c-fos and mCherry in the mPFC of the four groups of mice. Asterisks indicate neurons that co-express mCherry and c-fos; arrowheads indicate mCherry-expressing cells without detectable c-fos expression. Scale bar, 100 μm or 20 μm. **F** Immunostaining analyses show that the density of mCherry-infected neurons co-labeled with c-fos in the mPFC is significantly increased after the CNO injection (CNO effect: $F_{1, 20} = 17.57$, $p < 0.001$; two-way ANOVA). **G**, **H** Activation of PNs in the mPFC reverses ES-induced deficits of temporal order memory (**J**, CT-Veh *vs*. ES-Veh: $p = 0.003$, ES-Veh *vs*. ES-CNO: $p = 0.038$, Bonferroni's test) and spatial working memory (**K**, SA: CT-Veh *vs*. ES-Veh: $p = 0.002$; ES-Veh *vs*. ES-CNO: $p = 0.008$, Bonferroni's test; SAR: CT-Veh *vs*. ES-Veh: $p = 0.003$, ES-Veh *vs*. ES-CNO: $p = 0.007$, Bonferroni's test). **I** Experimental timeline of the behavioral tests, CNO injection, and brain tissue acquisition after CamkIIa-Gq and DIO-Gi viral infection in adolescent PV-Cre mice. **J** Representative images showing the expression of mCherry and c-fos in the mPFC of the four groups of mice. CNO increases the number of activated PNs (co-expressing mCherry and c-fos) in stressed (ES-Veh *vs*. ES-CNO, $p < 0.001$, Bonferroni's test) mice. Asterisks indicate neurons that co-express mCherry and c-fos; arrowheads indicate mCherry-expressing cells without detectable c-fos expression. Scale bar, 20 μm. **K** Representative images showing the expression of PV and c-fos in the mPFC of the four groups of mice. PVI activity was inhibited in control mice after CNO administration and was reduced in ES-exposed vehicle mice (CT-Veh *vs*. CT-CNO, $p = 0.028$; CT-Veh *vs*. ES-Veh, $p \leq 0.023$, Bonferroni's test). Asterisks indicate neurons that co-express PV and c-fos; arrowheads indicate PV-expressing cells without detectable c-fos expression. Scale bar, 20 μm. **L** In the temporal order memory test, the inhibition of mPFC PVIs blocked the effects of the activation of PNs (ES-Veh *vs*. ES-CNO: $t_{10} = 0.048$, $p = 0.963$, unpaired *t*-test) on reversing the temporal order memory impairment induced by ES (CT-Veh *vs*. ES-Veh: $t_{13} = 4.556$, $p < 0.001$, unpaired *t*-test). **M** In the Y-maze spontaneous alternation test, a significant main effect of stress was observed on the SA ($F_{1, 27} = 4.859$, $p = 0.036$), indicating the absence of the reversal effects of PN activation after PVI inhibition. In addition, CNO significantly increased AAR ($F_{1, 27} = 11.72$, $p = 0.002$) and decreased SAR ($F_{1, 27} = 8.421$, $p = 0.007$). Data are represented as mean ± SEM. $^{*}p < 0.05$, $^{**}p < 0.01$ and $^{***}p < 0.001$, unpaired *t*-test or Bonferroni's *post hoc* test; $^{\#}p < 0.05$, paired *t*-test. $^{\&}p < 0.05$, stress effect of two-way ANOVA. $^{\$\$}p < 0.01$, $^{\$\$\$}p < 0.001$, CNO effects in two-way ANOVA. AAR alternative arm return, CNO clozapine-N-oxide, CT control, ES early-life stress, mPFC medial prefrontal cortex, PND postnatal day, PVI parvalbumin-expressing interneuron, SA spontaneous alternation, SAR same arm return, Veh vehicle, VGluT1 vesicular glutamate transporter-1. See also Figs. S9–S14.

and percentage (S17M) of PVIs co-labeled with c-fos was significantly reduced by DREADDs. In the TOM task, compared with stressed mice that received antalarmin treatment and exhibited intact temporal order memory, CNO mice could not discriminate between the "remote" and "recent" objects and spent a significantly lower percentage of time exploring the "remote" object (Figs. 5U and S17L), indicating that the effect of antalarmin on reversing the ES-induced TOM impairment (see Fig. 5N) was blocked by mPFC PVI inhibition. Taken together, these pharmacological experiments indicate that CRHR1 blockade could successfully reverse ES-induced temporal order memory deficits by restoring mPFC PVI activity, supporting the therapeutic potential of antalarmin for treating ES-related cognitive impairments.

Environmental enrichment alleviates early-life stress-induced cognitive deficits and PN/PVI activity reduction in adolescent mice

In addition to pharmacological intervention, we also tested whether EE, a commonly used nonpharmacological intervention for animals exposed to ES, could reverse the negative effects of ES on adolescent mice. Stressed and control mice were exposed to enriched or standard housing environments for three weeks after weaning (PND21-42) and were then subjected to the TOM task (Figs. 6A, B and S18A, B). As shown in Fig. 6C, despite the lack of significant main effects and interactions in the two-way ANOVA, only the stressed mice housed in a standard environment failed to distinguish the "remote" object from the "recent" object, while the mice in the other three groups exhibited intact recognition memory, which indicates that EE partially reversed the ES-induced temporal order memory deficits.

We then investigated the neural correlates underlying the cognition-improving effects of EE by measuring the activity of PNs and PVIs in the mPFC. We found that significant effects of the stress × environment interaction were observed on the percentage and density of neurogranin^{+} cells that were c-fos^{+} (indicative of PN activity) in the mPFC (Figs. 6D, E, and S18C). Specifically, ES significantly reduced neurogranin^{+} neuron activity, which was reversed by environmental enrichment. Similar to the results for PNs, we also observed significant effects of the stress × environment interaction on the density and percentage of PVIs that were c-fos^{+} (Figs. 6G, H, and S18D). ES significantly reduced PVI activity, and EE significantly upregulated the activity of PVIs in stressed mice. Importantly, the discrimination indices in the temporal order memory test were significantly correlated with both the density of activated PNs (Fig. 6F) and PVIs (Fig. 6I) in the mPFC.

These data support the beneficial effects of EE on alleviating ES-induced temporal order memory deficits and reducing the activity of PNs and PVIs.

DISCUSSION

In this study, we examined whether and how mPFC PVIs causally mediate ES-induced cognitive deficits in adolescent mice. We first showed that exposure to a resource-scarce environment early in life led to a selective reduction in PVI activity in the mPFC in adolescent male mice, along with cognitive deficits in temporal order memory and spatial working memory. Ablating or inhibiting PVIs in the mPFC in adolescent mice phenocopied the deficits observed in ES-exposed mice, and activating PVIs rescued ES-induced cognitive deficits, supporting the causal relationship between PVI activity and cognitive deficits in mice exposed to ES. To understand how ES reduces PVI activity, we demonstrated that ES upregulated CRHR1 (mainly expressed in PNs) and reduced the activity of local PNs and their excitatory inputs onto PVIs. Importantly, genetic manipulation experiments revealed that CRHR1 and PNs causally contributed to cognitive deficits, which required the activation of PVIs. These results suggest that the pathophysiological mechanisms underlying cognitive deficits induced by ES may involve the prefrontal CRHR1-PN-PVI pathway in adolescent male mice. Finally, our intervention experiments

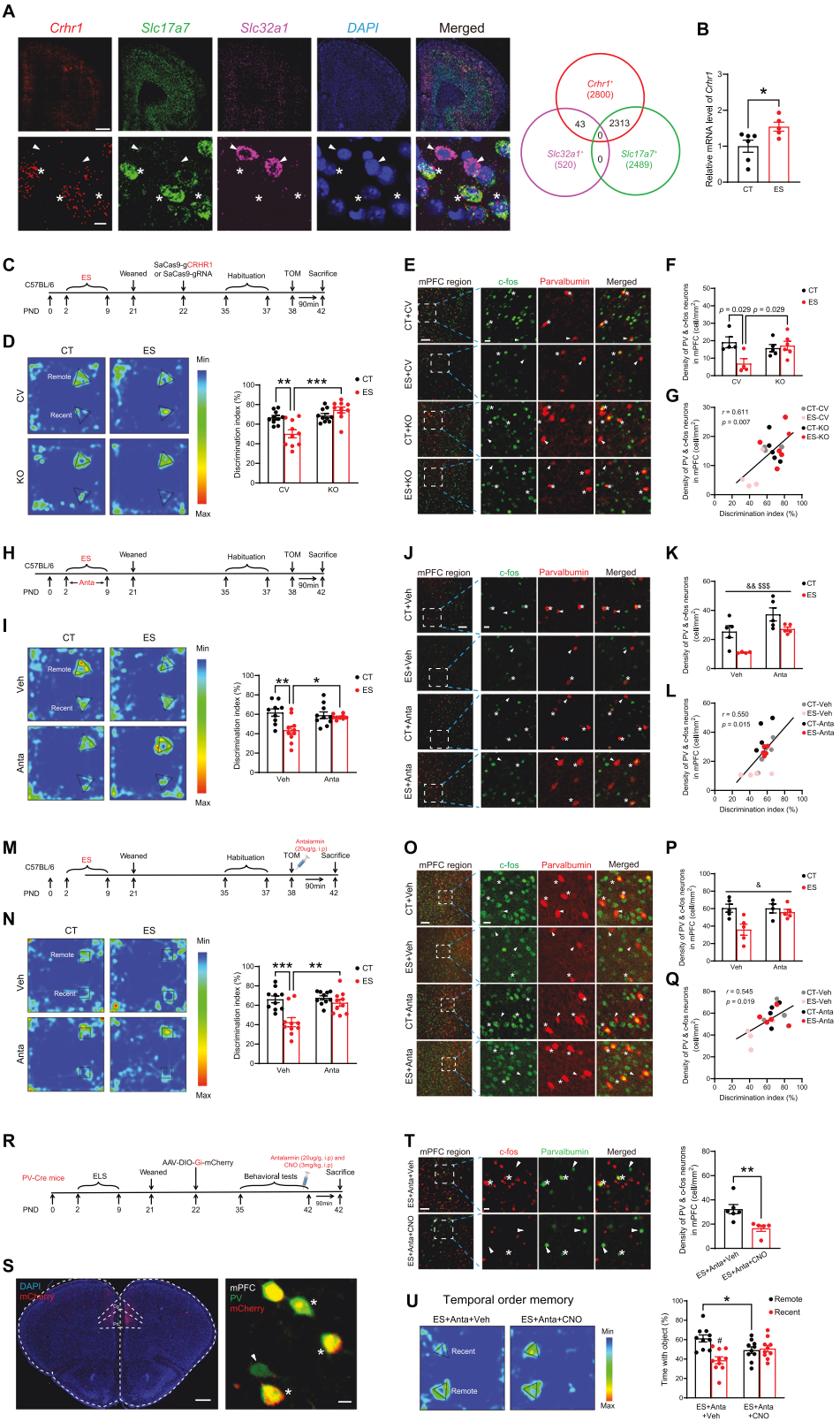

revealed the beneficial effects of pharmacological (antalarmin) and nonpharmacological (EE) treatment on ES-induced cognitive deficits and mPFC PVI activity, providing insights into the early treatment and prevention of cognitive impairments in individuals with stress-related psychiatric diseases.

Although our group and other research groups have extensively studied the effects of ES on cognition [4, 51], several recent studies have begun to examine this issue in adolescent rodents. Studies with maternal separation or deprivation models reported that ES impaired spatial learning and memory in the Morris water maze

Fig. 5 CRHR1 downregulation reverses early-life stress-induced cognitive deficits in adolescent male mice by restoring PVI activity in the medial prefrontal cortex. A *Crhr1* expression in excitatory and inhibitory neurons in the mPFC of adolescent mice. Left panel, representative (top, scale bar, 50 μm) and magnified (bottom, scale bar, 10 μm) images showing the mRNA expression of *Crhr1*, *Slc32a1*, and *Slc17a7*. Right panel, numbers of neurons that co-express *Crhr1* and *Slc32a1*, *Crhr1* and *Slc17a7*, *Slc32a1* and *Slc17a7*, and *Crhr1*, *Slc32a1*, and *Slc17a7*. Numbers in parentheses indicate the total number of neurons expressing the corresponding mRNA. **B** ES upregulated *CRHR1* mRNA level in mPFC of adolescent male mice ($t_9 = 2.489$, $p = 0.035$, unpaired *t*-test). **C**, **H**, and **M** Experimental timeline in the behavioral tests and brain tissue acquisition after CRHR1 knockout in mPFC (**C**), antalarmin administration during ES exposure (**H**), or acute antalarmin treatment (**M**) in C57BL/6 mice. **D**, **I**, and **N** ES-induced deficits of temporal order memory were reversed by mPFC CRHR1 deletion (**D**, CT-CV *vs*. ES-CV: $p = 0.002$, ES-CV *vs*. ES-KD: $p < 0.001$, Bonferroni's test), chronic antalarmin administration during PND2-8 (**I**, CT-Veh *vs*. ES-Veh: $p = 0.003$, ES-Veh *vs*. ES-Anta: $p = 0.042$, Bonferroni's test), and acute antalarmin treatment (**N**, CT-Veh *vs*. ES-Veh: $p = 0.002$, ES-Veh *vs*. ES-Anta: $p = 0.002$, Bonferroni's test). **E**, **J**, and **O** Representative images showing the expression of c-fos and PV in the mPFC of four groups. Asterisks indicate neurons that co-express c-fos and PV; arrowheads indicate PV-expressing cells without detectable c-fos expression. Scale bar, 100 μm or 20 μm. **F**, **K**, and **P** The effects of CRHR1 blockade on the reduction in PVI activity reduction induced by ES. **F**, **K** The negative effects of ES were reversed by CRHR1 deletion in the mPFC (**F**, CT-CV *vs*. ES-CV: $p = 0.029$, ES-CV *vs*. ES-KD: $p = 0.029$; unpaired *t*-test) or acute antalarmin treatment (**K**, CT-Veh *vs*. ES-Veh: $p = 0.001$; ES-Veh *vs*. ES-Anta: $p = 0.007$; Bonferroni's test). **P** Chronic antalarmin administration during PND2-8 upregulated the density of PVIs co-labeled with c-fos reduced by ES ($F_{1, 15} = 17.82$, $p < 0.001$, two-way ANOVA). **G**, **L**, and **Q** Correlations between mPFC PVI activity and the discrimination index in the temporal order memory test across all animals in each experiment. **R** Experimental timeline of the behavioral tests, CNO and antalarmin injection, and brain tissue acquisition after DIO-Gi viral infection in adolescent PV-Cre mice. **S** Left panel, representative image showing region-specific expression of mCherry in the mPFC; right panel, representative the image showing that the majority of PVIs express hM4Di in the mPFC. Asterisks indicate neurons that co-express mCherry and PV; arrowheads indicate PV-expressing cells without detectable mCherry expression. Scale bar, 500 μm or 10 μm. **U** In temporal order memory test, the inhibition of mPFC PVIs blocked the effects of an acute injection of antalarmin on reversing the temporal order memory impairment induced by ES (ES-Anta-Veh *vs*. ES-Anta-CNO: $t_{18} = 2.464$, $p = 0.024$, unpaired *t*-test; ES-Anta-Veh: $t_9 = 3.122$, $p = 0.012$, ES-Anta-CNO: $t_9 = 0.242$, $p = 0.815$, paired *t*-test). **T** Representative images showing the expression of PV and c-fos in the mPFC of the two groups of mice. PVI activity was inhibited in stressed mice acutely injected with of antalarmin after CNO administration ($t_9 = 4.898$, $p < 0.001$, unpaired *t*-test). Asterisks indicate neurons that co-express PV and c-fos; arrowheads indicate PV-expressing cells without detectable c-fos expression. Scale bar, 100 μm or 20 μm. Data are represented as mean ± SEM. $^{*}p < 0.05$, $^{**}p < 0.01$ and $^{***}p < 0.001$, Bonferroni's *post hoc* test; $^{\&}p < 0.05$, $^{\&\&}p < 0.01$, for the effect of stress from two-way ANOVA; $^{\$\$\$}p < 0.001$, for the effect of the drug from two-way ANOVA. Anta antalarmin, Cg cingulate cortex, CNO clozapine-N-oxide, CT control, CV control virus, ES early-life stress, KO knockout, mPFC medial prefrontal cortex, PND postnatal day, PrL prelimbic cortex, PVI parvalbumin-expressing interneuron, Veh vehicle. See also Figs. S15–S17.

test [37], novel object recognition memory test [52], and temporal order memory test [53] in adolescent rodents. To our knowledge, only one study has used the LBN paradigm and found that exposure to LBN during PND4-11 impaired spatial object recognition in adolescent male mice [7]. Extending these studies, which usually adopted one cognitive task, we tested adolescent mice exposed to LBN on a larger battery of cognitive tasks, including temporal order memory, spatial working memory, novel object recognition, and spatial object recognition. We found that ES-induced cognitive impairments were already present in adolescence. Intriguingly, unlike several studies showing both cognitive and emotional deficits following ES [8, 28, 37] while consistent with one previous study [54], here, we observed cognitive deficits only, without significant alterations in anxiety-like, depression-like, or social behaviors. Some LBN studies have reported emotional alterations in adolescent animals, such as a reduced sucrose preference [55], increased immobility time in the FST [56, 57], and increased anxiety-like behaviors [58, 59]. The inconsistency among these studies may be related to differences in the species (mouse or rat), stress mode, and age of stress exposure. Together, our observation of ES-induced cognitive deficits in adolescent mice provides further evidence that the LBN paradigm is a valid model for the early onset of cognitive impairments, one of the core symptoms of psychiatric disorders, and for studying the underlying neural mechanisms involved.

Considering the pivotal role of PVIs in mPFC-dependent cognitive behaviors and their prolonged maturation during adolescence, we hypothesized that PVIs may causally mediate ES-induced cognitive deficits in adolescent mice. As mentioned in the Introduction, previous studies have largely focused on the effects of ES on the number (density) of PVIs or the expression of *PV* mRNA or PV protein, some of which have reported down-regulation in adolescent animals [9, 23–25]. To our knowledge, direct evidence is still lacking regarding how ES affects the functional activity of prefrontal PVIs. One recent study revealed that ES (maternal separation and early weaning) decreased the evoked action potentials of mPFC GABAergic neurons in adult mice [60]; however, the types of interneurons that are affected and whether such effects emerge in adolescence remain unclear. In this study, we reported for the first time that ES significantly decreased mPFC PVI activity in adolescent male mice based on our c-fos colocalization and electrophysiological findings. Compared with that in the hippocampus, the ES-induced reduction in PVI activity in the mPFC is relatively specific, which is consistent with a previous report showing that maternal separation significantly reduced PV protein levels in the mPFC but not in the hippocampus of adolescent rats [9] and may be related to the delayed maturation of prefrontal PVIs during adolescence [21].

Moreover, regarding the link between reduced mPFC PVI activity and cognitive deficits in adolescent mice exposed to ES, previous studies using adult animals (not adopting the ES models) have provided supporting evidence. For example, the inactivation of prefrontal PVIs impaired prefrontal-dependent cognitive abilities, including spatial working memory, reversal learning [61], and rule-shift learning [16, 17, 62], whereas enhancing the activity of PVIs in the mPFC could alleviate these cognitive deficits in various animal models [19, 63, 64]. Two recent studies using adolescent animals also suggested the crucial involvement of mPFC PVIs in cognitive behaviors. One study revealed that sustained inhibition of prefrontal PVIs activity during adolescence disrupted cognitive flexibility in adult mice [18]. Another study reported that the selective activation of prefrontal PVIs during adolescence rescued deficits in novel object recognition induced by chronic MK801 treatment [65]. Here, by manipulating mPFC PVI functional activity through chemogenetic and optogenetic methods, we found that ablating or inhibiting PVIs in adolescent mice mimicked the deficits observed in ES-exposed mice and that activating PVIs rescued ES-induced cognitive deficits. These results provide causal evidence that mPFC PVI activity mediates the cognitive deficits induced by ES.

We targeted the CRH-CRHR1 system and PNs to understand the mechanisms by which ES reduces the functional activity of PVIs during adolescence. The CRH-CRHR1 system plays a crucial role in the adverse effects of ES, and recent clinical and animal studies have highlighted its association with PFC-dependent cognitive dysfunction [31, 35]. Numerous studies have reported that ES

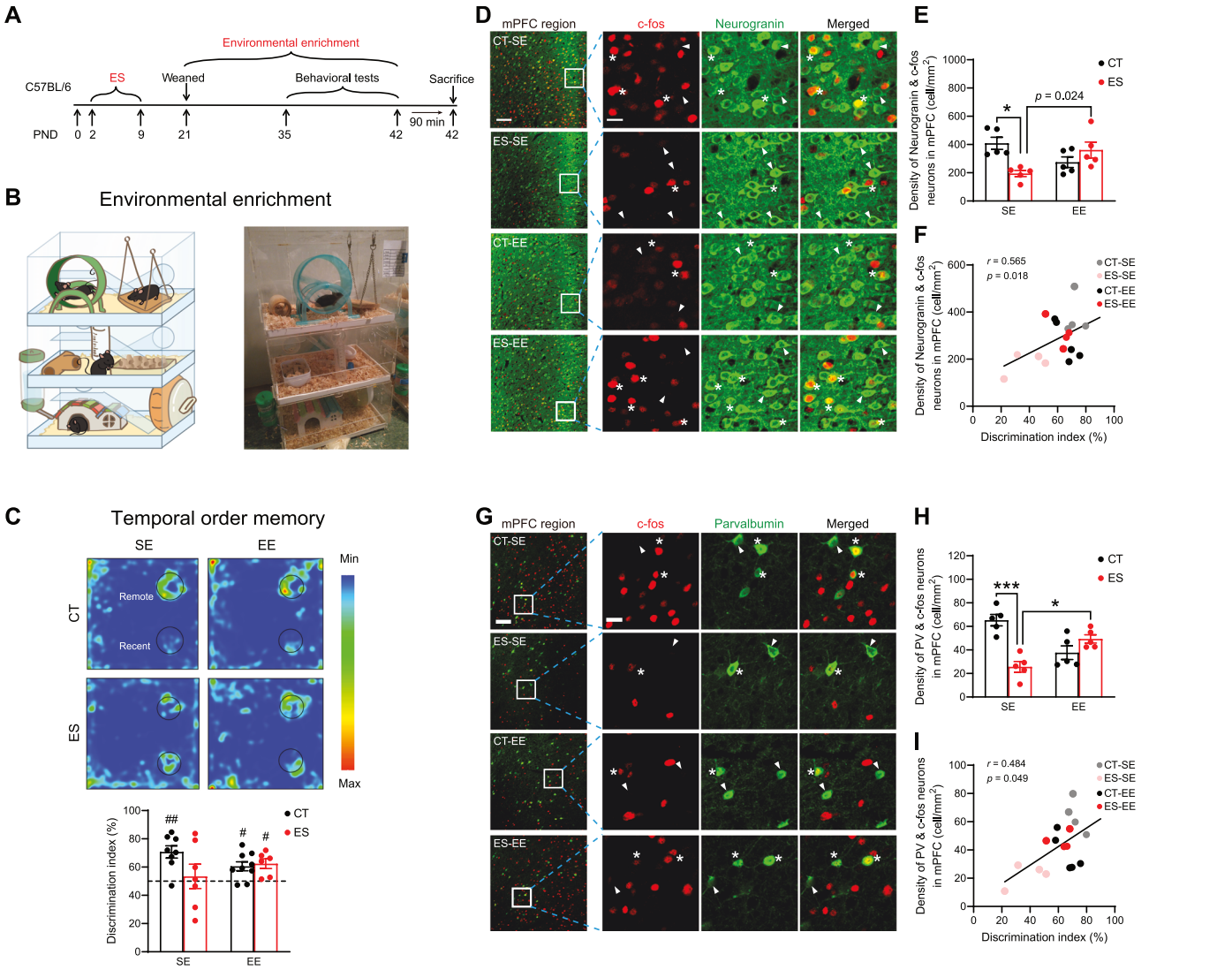

Fig. 6 Environmental enrichment alleviates early-life stress-induced cognitive deficits through activation of prefrontal PNs and PVIs in adolescent male mice. A Experimental timeline of EE exposure, behavioral tests, and brain tissue acquisition after ES. **B** A schematic illustration (left panel) and a photograph (right panel) of the enriched housing environment. **C** EE partially reversed the ES-induced temporal order memory deficits. Only the stressed mice in the standard housing environment failed to distinguish the "remote" object from the "recent" object (ES-SE: $t_6 = 0.396$, $p = 0.706$, paired *t*-test), while the mice in the other three groups exhibited intact temporal order memory (CT-SE: $t_7 = 4.818$, $p = 0.002$; CT-EE: $t_8 = 3.316$, $p = 0.011$; ES-EE: $t_5 = 3.609$, $p = 0.015$; paired *t*-test). **D** Representative images showing the expression of c-fos and neurogranin in the mPFC of the four groups. Asterisks indicate neurons that co-express c-fos and neurogranin; arrowheads indicate neurogranin-expressing cells without detectable c-fos expression. Scale bar, 100 μm or 20 μm. **E** ES significantly reduced neurogranin$^+$ neuron activity ($p = 0.013$, Bonferroni's test), which was reversed by environmental enrichment ($t_8 = 2.774$, $p = 0.024$ unpaired *t*-test). **F** The correlation between mPFC PN activity and the discrimination index in the temporal order memory test across all animals. **G** Representative images showing the expression of c-fos and PV in the mPFC of the four groups. Asterisks indicate neurons that co-express c-fos and PV, while arrowheads indicate PV-expressing cells without detectable c-fos expression. Scale bar, 100 μm or 20 μm. **H** ES significantly reduced PVI activity ($p < 0.001$, Bonferroni's test), which was reversed by environmental enrichment ($p = 0.017$, Bonferroni's test). **I** The correlation between mPFC PVI activity and the discrimination index in the temporal order memory test across all animals. Data are represented as mean ± SEM. $^*p < 0.05$, $^{**}p < 0.01$ and $^{***}p < 0.001$, Bonferroni's *post hoc* test; $^{\#}p < 0.05$ and $^{\#\#}p < 0.01$, paired *t*-test. CT control, ES early-life stress, EE environmental enrichment, mPFC medial prefrontal cortex, PND postnatal day, PVI parvalbumin-expressing interneuron, SE standard environment. See also Fig. S18.

reduces the functional activity of PNs [60, 66] and impairs their structural plasticity (e.g., dendritic retraction and spine loss [27, 67]) in adult animals. Considering that CRHR1 is mainly expressed in excitatory neurons rather than inhibitory neurons in the mPFC ([42] and Fig. 5A), we speculate that ES may first act on CRHR1 on PNs, reducing PN neuronal activity and excitatory inputs to PVIs, leading to decreased activity of PVIs and ultimately leading to cognitive impairment in adolescent mice. This speculation was supported by the following results: (1) ES upregulated CRHR1 expression, downregulated PN and PVI activity, and decreased excitatory inputs onto PVIs from local PNs. (2) Overexpression in CRH and genetic knockout of CRHR1 in the mPFC mimicked and restored the ES-induced cognitive impairment and PVI activity reduction, respectively. (3) Inhibition of mPFC PNs mimicked the ES-induced TOM deficits, and activation of mPFC PNs reversed ES-induced cognitive impairments. (4) The reversal effects of CRHR1 knockout and PN activation could be blocked by inhibiting mPFC PVI activity, indicating that PVIs play indispensable roles in CRHR1- or PN-mediated cognitive deficits induced by ES. Together, our series of

experiments demonstrate how ES reduces PVI activity in the mPFC of adolescent male mice. Based on current results, we do not know yet how PVI activity reduction mediates ES-induced cognitive deficits. We carried out a chemogenetic experiment (simultaneously activating PVIs and inhibiting PNs) to partly address this question, showing that mPFC PVIs can improve cognitive behaviors in ES-exposed mice when local PNs were inhibited, which suggests that the improving effects of PVIs could be independent of local PN activity. Current literature suggests that the functions of PVIs go beyond basic PVI-PN microcircuits and play a critical role in complex neuronal network modulation [68, 69]. As our chemogenetic manipulation does not abolish PN activity completely (see Fig. S10B), we speculate that PVIs may interact with the PNs that were not inhibited or with other PVIs [70], possibly at the neuronal network level, to improve cognition.

It is noteworthy that while our study focuses on the local CRHR1-PN-PVI pathway in the mPFC, there are external CRH-positive neurons projecting to the mPFC PNs and external excitatory neurons projecting to the mPFC PVIs. First, CRH-positive neurons are widely distributed in cortical and subcortical brain regions [71, 72]. Our data (via viral tracing) demonstrated that the mPFC receives external projections from CRH-positive neurons in multiple stress-related brain regions, such as basolateral amygdala, anteromedial thalamic nucleus (Fig. S19). Intra-mPFC CRH microinjection has been found to impair temporal order memory in adult male mice [34], which links mPFC CRH increases to cognitive deficits, but did not distinguish the various sources of CRH. Our CRH overexpression experiment shows that CRH released by the mPFC CRH-positive neurons is sufficient to mimic the detrimental effects of ES on PN/PVI activity and cognition. Future studies are warranted to examine whether CRH-positive neurons in the brain regions projecting to the mPFC also contribute to ES-induced cognitive deficits. Second, regarding the excitatory inputs from PNs to PVIs, recent whole-brain imaging results reveal that PVIs in the mPFC not only receive projections from local PNs (about 10%) but also receive a significant number of projections from PNs outside the mPFC [73]. In this study, we focused on the local PNs, because 10% of projections are from local PNs, which still exceed projections from the majority of individual brain regions (e.g., hippocampus, amygdala) and constitute a significant regulator of mPFC PVI activity. Future studies should carefully disentangle to what extent the mPFC PVI activity reduction we observed could be attributed to CRH-positive or excitatory neurons from brain areas outside the mPFC.

For the treatment of cognitive impairment in clinical practice, the efficacy of current first-line therapeutic drugs and nonpharmacological treatments such as psychotherapy and physical therapy (e.g., rTMS) is limited [5], which warrants the development of effective therapies for early intervention [30]. Here, by targeting ES-induced cognitive deficits and reducing mPFC PVI activity, we examined the efficacy of pharmacological (i.e., antalarmin, a CRHR1 antagonist) and nonpharmacological (i.e., environmental enrichment) interventions. Several clinical trials on drugs targeting the CRH-CRHR1 system have been conducted; these trials have largely focused on improving symptoms of depression and anxiety, not cognition, and have ended in failure [74, 75]. Our series of studies have consistently shown the cognition-improving effects of antalarmin, such as PFC-dependent temporal order memory and spatial working memory [27, 40], and hippocampus-dependent memory functions [49, 76], in animal models of early-life stress in adulthood. In this study, we found that either co-administration or acute intraperitoneal injection of the CRHR1 antagonist antalarmin reversed the ES-induced cognitive impairment and decrease in mPFC PVI activity in adolescent mice. These results highlight the therapeutic potential of CRHR1 antagonism on cognitive dysfunctions (compared with emotional symptoms) in individuals with stress-related psychiatric disorders and support its potential application in adolescent individuals.

Compared with medications, nonpharmacological interventions for psychiatric disorders have advantages in terms of fewer adverse effects and better acceptability. EE is a commonly used nonpharmacological intervention for animals exposed to ES and has beneficial effects on ES-induced behavioral and neural changes [36, 77]. Regarding cognitive impairment, two studies using maternal separation have reported the beneficial effects of EE during adolescence (i.e., reversal learning [37] and spatial working memory [38]). Our study revealed that the cognitive impairment caused by LBN can also be reversed by EE. We further examined the underlying mechanisms of the effects of EE and showed that EE significantly upregulated mPFC PN and PVI activity. Inhibition of PVIs has been found to block the improvement of cognitive deficits by EE [65, 78]. Together, these results indicate that PVIs may mediate the effects of EE on ES-induced cognitive deficits. Previous studies have shown that EE significantly downregulates the expression of the *Crh* mRNA in the hippocampus of a rat model of absence epilepsy [79] and decreases the expression of the *Crhr1* mRNA in the amygdala of C57BL/6 mice [80]. Thus, the effects of EE we observed might be related to the normalization of the ES-induced upregulation of the CRH-CRHR1 system.

Importantly, some limitations of our study warrant consideration. First, we tested only adolescent male mice in this study. In adolescent female mice, we have recently revealed that ES similarly impairs their cognitive functions, including NOR, SOR, and TOM, similar to our current findings in adolescent male mice [81]. Acute administration of antalarmin was found to restore NOR and SOR, but not TOM, impairments in adolescent female mice. Unfortunately, we did not test mPFC PVI activity in that study. Further research is needed to systematically investigate whether the mPFC PVI mechanisms we observed in male mice could be generalized to female mice. Second, although our c-fos experimental results indicated that multiple interventions reversed ES-induced cognitive deficits by restoring PVI activity, we did not verify the PVI results with electrophysiological recordings in these experiments, which should be pursued in future studies. Third, for the involvement of CRH-CRHR1 signaling in the EE experiment, we did not provide evidence of whether and how EE affects mPFC CRH-CRHR1 signaling in ES-exposed mice. Future studies could carry out genetic or pharmacological experiments to systematically examine whether the CRH-CRHR1 system causally mediates EE intervention on ES-induced cognitive deficits.

In summary, our study revealed the crucial role of prefrontal PVIs, along with PNs and CRHR1, in mediating cognitive deficits induced by early-life stress in adolescent male mice. Our findings also highlight that prefrontal PVI activity could serve as a potential treatment or intervention target to ameliorate the cognitive impairments of individuals with stress-related psychiatric disorders.

MATERIALS AND METHODS

Animals

Adult C57BL/6 (10–12 weeks old) male and female mice were purchased from Vital River Laboratories (Beijing, China). The mice were transferred to individually ventilated cages (IVC) and 3–4 mice were housed normally. Pvalb$^{tm1(cre)Arbr}$/J (PV-Cre) mice express Cre recombinase in parvalbumin-expressing interneurons (PVIs) [82]. Gt (ROSA)26Sor$^{tm14(CAG-tdTomato)Hze}$/J (Ai14) mice exhibit robust tdTomato fluorescence following Cre-mediated recombination [83]. Tg (Camk2a-cre)$^{T29-1Stl}$/J (CamkIIa-Cre) mice express Cre recombinase in pyramidal neurons (PNs) in the forebrain [84]. The *Crh*$^{tm1(cre)Zjh}$/J (CRH-Cre) mice express Cre recombinase in CRH-positive neurons. All transgenic mice were purchased from the Jackson Laboratory (CA, USA) and maintained fully back-crossed onto C57BL/6 mice, and adult male heterozygous mice were used. No statistical methods were used to estimate the sample size. Sample sizes in each group were chosen based on previous studies ($n \geq 6$ for behavioral tests; $n \geq 5$ for genetic manipulation tests; $n \geq 4$ for molecular tests).

For breeding, male and female mice were mated at a 1:2 ratio for 2 weeks and separated. Pregnant females were monitored daily for pup delivery, and the day of parturition was defined as postnatal day 0 (PND0). Only male offspring were used in subsequent experiments. All mice were on under a 12-h light/dark cycle (lights on at 8:00 a.m.) at a constant temperature (23 ± 1 °C) with plenty of food and water. All experiments were approved by the Peking University Committee on Animal Care, and they were performed in compliance with the NIH's Guide for the Use and Care of Laboratory Animals.

Early-life stress paradigm

The limited nesting and bedding paradigm was used as an early-life stressor and was conducted as previously described [49]. The procedure was as follows: At PND2, the number of pups per cage was adjusted to ensure that each cage contained 6–8 pups with a male-to-female ratio of 1:1. The control dams received 500 ml of sawdust bedding and 4.8 g of nesting material (2 squares of nestlets, Ancare, New York, USA), while in the "stress" cages, the dams were provided with a fine-gauge aluminum mesh platform (McNichols, Tampa, FL, USA) with 200 ml of corncob bedding on the bottom to collect the droppings. A limited amount of nesting material [1/2 square (1.2 g) of nestlets] was placed on top of the mesh. After one week of stress treatment (PND2–9), all the mice were returned to the standard environment. Male offspring were weaned at PND21 and housed in groups of 3–4 per cage for further study. Siblings were split into groups equally whenever possible, with 1–3 pups per dam in each group.

Behavioral assays

A battery of behavioral tests, including tests of cognitive behaviors, anxiety-like behaviors, depression-like behaviors, and social approach, were performed in adolescent male mice (PND35-42) between 09:00 and 15:00 as described previously [27, 85]. Mice were handled for at least 3 days prior to behavioral testing. Behavioral data in the open field, elevated plus maze, and light–dark box tests were automatically analyzed using ANY-maze 7.0 (Stoelting, Wood Dale, IL, USA). The results of the remaining behavioral tests were scored by an experimenter who was blinded to the experimental conditions. For object recognition tests, mice showing the total probe time with two objects in either the acquisition or test phase below 10 s would be excluded from statistical analyses.

Temporal order memory test. The temporal order memory (TOM) test, which relies on the medial prefrontal cortex (mPFC), was used to assess the ability of the animals to differentiate between two familiar objects presented at different time intervals [86]. The test was performed in an open field arena illuminated at 10 lux and included 3 trials with a 1-h intertrial interval (ITI). The first two trials were the acquisition trials in which two identical triangular prisms or triangular pyramids were placed in the arena and the animals were allowed to freely explore the arena for 10 min. In the test phase, a triangular prism (the "remote" object) and a triangular pyramid (the "recent" object) were placed in the arena. During the 10 min test phase, the discrimination index was calculated as: 100% × time spent probing the "remote" object /time spent probing both objects.

Novel object recognition test. The novel object recognition (NOR) task was designed to assess recognition memory based on familiarity with the object itself, which depends on several brain regions, including the perirhinal cortex, the hippocampus, and mPFC [87]. The NOR test was also performed in the open field arena, illuminated at 10 lux, and consisted of 2 trials separated by an ITI of 1 h. During the acquisition phase, two identical cubes were presented. In the test phase, one of the cubes (the "familiar" object) was replaced with a hexagonal column (the "novel" object). During the 10 min test phase, the discrimination index was calculated as: 100% × time spent probing the "novel" object /time spent probing both objects.

Spatial object recognition test. The spatial object recognition (SOR) task was designed to assess the animals' ability to detect changes in the location of familiar objects, which depends on the hippocampus [88]. The test was conducted in the open field arena with a 10 lux illumination and consisted of two acquisition trials and one test trial with 1-h ITI. During the first two acquisition trials, two identical objects (cylinders) were placed approximately 15 cm apart. One hour later, one object was moved diagonally (the "displaced" object), and the other object remained in its original position (the "stationary" object). During the 10-min test phase, the discrimination index was calculated as: 100% × time spent probing the "displaced" object /time spent probing both objects.

Y-maze spontaneous alternation test. The Y-maze spontaneous alternation task was designed to assess spatial working memory [89]. The Y-maze apparatus consisted of gray polyvinyl chloride with three symmetrical arms ($30 \times 10 \times 15$ cm^3, 10 lux) and spatial cues surrounding the maze. Mice were placed at the end of one arm and allowed to explore freely for 8 min. The percentage of spontaneous alternations (SA: A→B→C), alternative arm returns (AAR: A→B→A), and same arm returns (SAR: A→A) were recorded manually.

Open field test. The open field test was performed in a gray polyvinyl chloride chamber (50 cm × 50 cm × 50 cm) with smooth interior walls and evenly illuminated at 60 lux. During the test, the mice were placed in one corner, facing the wall, and permitted to explore the environment freely for 10 min. The time spent in the center area of the open field (20 cm in diameter), the latency, and the number of entries to the center area were measured to reflect the animals' anxiety levels. The total distance traveled was also quantified.

Elevated plus maze test. The elevated plus maze test was performed in an elevated plus maze consisting of a central platform (5×5 cm^2) with two opposing open arms ($30 \times 5 \times 0.5$ cm^3, 40 lux) and two opposing closed arms ($30 \times 5 \times 15$ cm^3, 10 lux) extending from it in a plus shape. The maze was elevated 50 cm above the floor. Mice were individually placed in the center with their heads facing a closed arm and allowed to explore for 5 min. Time spent in the open arms, latency, and number of entries into the open arms were recorded.

Light–dark box test. The light–dark box test was performed in a plastic box containing a dark chamber ($15 \times 20 \times 25$ cm^3, 10 lux) and a brightly illuminated chamber ($30 \times 20 \times 25$ cm^3, 700 lux) connected by a 4-cm long tunnel. Mice were placed in the dark chamber facing the other chamber. The time spent in the light chamber during the 5 min test, the latency, and the number of entries to the light chamber were measured.

Tail suspension test. The test was conducted in a plastic enclosure (15 cm × 17 cm × 50 cm). Mice were suspended by the tail at the distal end for 6 min using a suspension hook. Mice were considered immobile when they were passively suspended and completely immobile. The total time spent immobile and the latency of immobilization were manually scored for each animal.

Forced swimming test. Mice were individually placed in a transparent cylinder (25 cm high, 10 cm diameter) filled with water to a depth of 18 cm and maintained at 25 ± 1 °C and tested for 6 min. After the test, the mouse was wiped dry with a towel and returned to its home cage. Mice were considered immobile if they did not make any active movements. The total immobility time was recorded and analyzed.

Sucrose preference test. Four days prior to the test, the mice were individually housed in their assigned cages with two bottles of tap water to avoid place preference bias. On the fourth day, two bottles containing a 1% sucrose solution were provided. The test began at 20:00, during which the mice were given one bottle containing a 1% sucrose solution and one bottle of water, and the weight of each bottle was recorded. The positions of the two bottles were changed every 12 h, and the bottle weights were recorded 24, 48, and 72 h later. Sucrose preference index (%) = 100 × (sucrose solution consumption)/(sucrose solution consumption + water consumption).

Social approach test. The social approach test was performed in a gray polyvinyl chloride chamber (50 cm × 50 cm × 50 cm) illuminated at 10 lux. Mice were acclimated to the chamber with an empty wire mesh cage in the center for 10 min. One hour later, a stranger mouse of the same sex and age (defined as a "tool" mouse) was placed in the empty wire mesh cage, and then the test mouse was placed in one corner facing the wall and allowed to explore freely for 10 min. The time spent interacting with the "tool" mouse was measured manually.

Immunohistochemistry and image analysis

Mice were anesthetized with 2,2,2-Tribromoethanol (250 mg/kg, i.p., T48402, Sigma–Aldrich) and transcardially perfused with 0.9% saline followed by 4% buffered paraformaldehyde. Then, mouse brains were dissected, post-fixed for 10–12 h at 4 °C in 4% buffered paraformaldehyde, and dehydrated in a 30% sucrose solution for 72 h at 4 °C. Using a cryostat

(Leica, Wetzlar, Germany), serial coronal sections of the mPFC (1.98 mm–1.54 mm from bregma) were obtained at 30-μm by a 180-μm interval.

For immunofluorescence staining, the sections were washed with 0.1 M PBS three times (10 min each time), and permeabilized with 0.3% Triton X-100 in 0.1 M PB three times for 10 min each, followed by incubation in a 1% normal donkey serum blocking solution at room temperature for 1 h. The following primary antibodies were used: goat anti-somatostatin (1:100, sc-7819, Santa Cruz), goat anti-parvalbumin (1:2000, PVG-213, SWANT), mouse anti-CamkIIa (1:1000, 22609, Abcam), mouse anti-parvalbumin (1:2000, PV-235, SWANT), mouse anti-VGluT1 (1:1000, 135511, Synaptic Systems), rabbit anti-parvalbumin (1:2000, PV-25, SWANT), rabbit anti-c-fos (1:1000, 2250S, Cell Signaling), rabbit anti-neurogranin (1:1000, 217672, Abcam), pig anti-c-fos (1:1000, 226005, Synaptic Systems) and rabbit anti-EGFP (1:1000, K009757P). After three rinses with 0.1 M PB containing 0.3% Triton X-100 (10 min each), the sections were incubated with secondary antibodies (Alexa Fluor 488-, 594- and or 647-conjugated donkey) diluted 1:500 in 1% normal donkey serum blocking solution for 2 h at room temperature. After three rinses with 0.1 M PB (10 min each), sections were mounted on slides and covered with Vectashield containing 4′,6-diamidino-2-phenylindole (DAPI; Vector Laboratories, Burlingame, CA).

For immunohistochemistry, the sections were washed with 0.1 M PBS three times (5 min each time) and treated with 3% hydrogen peroxide (10 min), followed by 1% normal goat serum (1 h). They were labeled with rabbit anti-parvalbumin (1:20000, PV-25, SWANT) or goat anti-somatostatin (1:200, sc-7819, Santa Cruz) antibody at 4 °C (overnight). The next day, the sections were rinsed and incubated with a biotinylated goat anti-rabbit or rabbit anti-goat secondary antibody (Zhongshan Golden Bridge Biotechnology, Beijing, China) at room temperature (2 h). After rinsing, sections were stained with the 3,3′-diaminobenzidine horseradish peroxidase color development kit (Zhongshan Golden Bridge, ZLI-9019, Beijing, China), transferred onto slides and coverslipped with mounting medium (Zhongshan Golden Bridge, ZLI-9516, Beijing, China).

For image analysis, brain sections were assigned random numbers so that investigators were blind to the experimental conditions. Images were obtained from 3 sections per animal with a 10× objective using an Olympus VS120-S6-W automated slide scanner (Olympus, Tokyo, Japan) and three subregions of the mPFC (Cg, PrL and IL) were defined as ROIs (Region of Interest) for analysis using NIH ImageJ software to determine the numbers of PVIs and somatostatin-expressing interneurons (SST-INs) in the mPFC. For the colocalization analysis, images of 3 brain sections from each animal were captured with a 20× objective using an Olympus FV1000 laser-scanning confocal microscope (Olympus, Tokyo, Japan). Images were acquired with a 20× objective from 3 sections per animal using an Olympus FV3000 laser-scanning confocal microscope (Olympus, Tokyo, Japan) to examine the optical density of VGluT1 at different distances from the soma of PVIs; for each group, 30–40 PVIs were chosen and Sholl analysis was performed using NIH ImageJ software. We first drew a circle (radius = 15 μm) around the center of PVI soma and then obtained the averaged optical density in the circle at different distances (step of 0.67 μm). Images were obtained with 10× objective using an Olympus VS200-S6-W automated slide scanner (Olympus, Tokyo, Japan) to validate the virus-injected or optical fiber-targeted regions. Images were adjusted for optimal brightness and contrast using FV10-ASW 4.2 software or OlyVIA 3.4.1 (Olympus, Tokyo, Japan).

Brain-slice preparation and electrophysiological recordings

Adolescent male PV::Ai14 mice (PND35-42) were rapidly anesthetized with isoflurane and decapitated. Brain slices (200 μm) containing the mPFC were obtained using standard techniques and incubated in artificial cerebrospinal fluid (ACSF)at room temperature (25 °C) for 1 h. The slices were then transferred to a recording chamber at room temperature (25 °C) and continuously perfused with an oxygenated-standard and ACSF heated at 30 °C that containing (in mM) 10 glucose, 125 NaCl, 5 KCl, 2 NaH_2PO_4, 2.6 $CaCl_2$, 1.3 $MgCl_2$, and 26 $NaHCO_3$ (pH: 7.3–7.4, osmolarity: 300–310 mOsm/kg), at a rate of 2 mL/min. Target mPFC PVIs were identified by tdTomato fluorescence using an Olympus BX51 microscope equipped with DIC optics, a water-immersion objective (×40 NA 1.1). Incremental current steps (0.5 s duration, 50 pA step size) were injected through the recording pipette to measure the evoked firing of PVIs. Recordings were obtained with an EPC-10 amplifier and Patchmaster software (HEKA Elektronik, Lambrecht/Pfalz, Germany). The signals were analyzed with Clampfit 10.3 (Molecular Devices, Union City, CA, USA).

The mPFC of PV-Cre mice was injected with a Cre-dependent CMV-DIO-mCherry virus, in addition to an AAV carrying the light-sensitive protein CamkIIa-ChR2-EGFP. Following a two-week period of expression, the mice were decapitated and their brains were removed. Immediately following the removal of the brain slices containing the mPFC were prepared with vibratome slices and the cells labeled with GFP were sought (Olympus BX51). The cells labeled with GFP were then manipulated for photo stimulation (473 nm, 12 mW, 10 ms pulses, 10 Hz, duration 3 min), with whole-cell membrane clamp recordings synchronized on cells with mCherry labels. The voltage of the mPFC cells was clamped at −70 mV, and the oEPSC was recorded to ascertain whether the connections between the PNs and PVIs in the mPFC were monosynaptic. Tetrodotoxin (TTX, 1 μM) was added sequentially to the sodium channel blocker 4-AP (1 mM), and changes in oEPSCs would suggest that the PN-PVI connection was monosynaptic. The oEPSC frequency and amplitudes were measured. To evaluate presynaptic release probability, paired pulses (duration of 10 ms) with an interval of 100 ms were delivered, and the paired-pulse ratio (PPR) was calculated as the EPSC2/EPSC1 amplitude ratio. Recordings were obtained with a Multiclamp 700B amplifier (Molecular Devices, USA) and Axon (Axon Enterprise, Inc, USA). Signals were analyzed with Clampfit 10.2 (Molecular Devices, Union City, CA, USA) and Mini Analysis Program (Synaptosoft).

Stereotaxic surgery and virus microinjection

Adolescent mice (PND22-23) were anesthetized with isoflurane (induction 2.5%, maintenance 1–1.5%) with perioperative meloxicam analgesia (3 mg/kg, i.p.) and placed in a stereotaxic frame (RWD Life Science Co., LTD, Shenzhen, China). The dorsal mPFC (i.e., Cg and PrL) were chosen for neuronal manipulation experiments, due to our focus on cognitive functions in mice. Mice received microinjections of viruses into the dorsal mPFC (Cg and PrL) through a glass micropipette (250 nL per side, 30 nL/min). The injection coordinates (relative to the bregma) were anterior +1.9 mm, lateral ±0.3 mm, and ventral −1.8 mm. The micropipette was left in the site for another 5 min. Mice were allowed to recover until the beginning of behavioral tests (PND35). In order to perform whole-cell recordings in PVIs in close proximity to optically activated pyramidal neurons, the adeno-associated virus (AAV) Cre-dependent CMV-DIO-mCherry and CamkIIa-hChR2(H134R)-EGFP viruses were injected into the mPFC of PV-Cre mice. The AAV of DIO-hM3Dq-mCherry (1.14×10^{13} genome copies/mL, Vigene Biotechnology, China), DIO-hM4Di-mCherry (3.00×10^{13} genome copies/mL, Vigene Biotechnology, China), DIO-eNpHR3.0-EYFP (1.81×10^{14} genome copies/mL, Vigene Biotechnology, China), flex-taCasp3-TEVp (3.04×10^{12} genome copies/mL, ObioTechnology, China), or ACSF was delivered bilaterally to the mPFC of male PV-Cre mice to perform whole-cell recordings of PVIs in close proximity to optically activated pyramidal neurons. For the manipulation of pyramidal neurons in the mPFC, an AAV virus of DIO-hM4Di-mCherry was bilaterally injected into the mPFC of male CamkIIa-Cre mice or AAV virus of CamkIIa-hM3Dq-mCherry (7.07×10^{13} genome copies/mL, Vigene Biotechnology, China) was bilaterally injected into the mPFC of male C57BL/6 mice. For simultaneous manipulation of mPFC PNs and PVIs, a mixture of CamkIIa-hM3Dq-mCherry and DIO-hM4Di-mCherry or a mixture of CamkIIa-hM4Di-mCherry and DIO-hM3Dq-mCherry were bilaterally injected into the mPFC of male PV-Cre mice. To overexpress *Crh* in the mPFC, a mixture of AAV-CRH-Cre-WPRE-hGH (CRH-Cre, 5.00×10^{12} particles/mL; ObioTechnology, China) and AAV-CAG-DIO-CRH-P2A-GFP (CRH_OE, 3.22×10^{13} particles/mL; Vigene Biosciences, Shandong, China) or a mixture of CRH-Cre and AAV2/9-CAG-DIO-GFP (3.23×10^{13} particles/mL, Vigene Biosciences) were bilaterally injected into the mPFC of male C57BL/6 mice. To achieve CRISPR-mediated deletion of *Crhr1*, an AAV vector carrying sgRNA targeting *Crhr1* (AAV2/9-CMV-SaCas9-U6-crhr1.gRNA, 7.22×10^{13} genome copies/mL, Vigene Biotechnology, China) and scrambled sgRNA (AAV2/9-CMV-SaCas9-U6-scrambled. gRNA, 4.13×10^{13} genome copies/mL, Vigene Biotechnology, China) was bilaterally injected into the mPFC of male C57BL/6 mice. To label the CRH-positive projection received by mPFC, a retrograde AAV vector (AAV2/retro-CAG-DIO-EGFP, 5.59×10^{12} genome copies/mL, BrainVTA, China) was bilaterally injected into the mPFC of male CRH-Cre mice.

Chemogenetic manipulation of neurons

Clozapine-N-oxide (CNO, HY-17366, MEC) was dissolved in 100% DMSO to a storage concentration of 20 mg/mL and stored at −20 °C. For the chemogenetic inactivation of PNs or PVIs and the double chemogenetic experiments, the storage solution of CNO was diluted to a working solution (0.3 mg/mL) and then the working solution of CNO was injected intraperitoneally (i.p. 3 mg/kg body weight) to hM4Di transfected mice 30 min prior to each behavioral test. For the chemogenetic activation of

PNs or PVIs storage solution of CNO (20 mg/mL) was diluted into a working solution (0.1 mg/mL) and then the working solution of CNO was administered intraperitoneally (i.p. 1 mg/kg) to hM3Dq transfected mice 30 min prior to each behavioral test. For vehicle groups, 3 mg/kg body weight of 1.5% DMSO or 1 mg/kg body weight of 0.5% DMSO were injected intraperitoneally in the inactivation and activation experiments, respectively. The higher dose (i.e., 3 mg/kg) was used for chemogenetic inhibition (Gi) experiments because our pilot experiments showed that 1 mg/kg of CNO was unable to inhibit neuronal activity, which might be due to some compensatory processes.

Optogenetic inactivation of PV-expressing interneurons

For the optogenetic inactivation of prefrontal PVIs, an AAV carrying DIO-eNpHR3.0-EYFP or DIO-EGFP was injected bilaterally into the mPFC of PV-Cre mice, and an optic-fiber cannula (200-μm -diameter; 0.37 NA) was implanted above the mPFC with −1.55-mm DV coordinate. Light was provided by a 594 nm laser diode (ThinkerTech, Nanjing, China). The light intensity at the fiber tip was measured with a light sensor (Thorlabs, Newton, NJ, USA). A 4–5 mW laser pulse (ON-OFF-ON-OFF, 2 min/section) was delivered during the behavioral test phase by a Master-8 pulse stimulator (AMPI, Jerusalem, Israel) through the optical fiber embedded in the mPFC.

RNAscope in situ hybridization

The expression of mRNAs in the mPFC was visualized using RNAscope (Advanced Cell Diagnostics). Following the manufacturer's instructions, mouse brains were rapidly dissected, dehydrated, and frozen. After cryoprotection, serial coronal sections (bregma 1.98–1.54 mm) of the mPFC at 15 μm thickness and 180 μm intervals were obtained using a cryostat (Leica), which were subsequently dried at −20 °C for 1 h and stored at −80 °C for up to one week. Then, slices were processed following the RNAscope protocol using a fluorescent multiplex reagent kit (ACD: 323100) and probes for *Crhr1* (Mm-Crhr1-C1; ACD, catalog #418011), *Slc32a1* (Mm-Slc32a1-C2; ACD, catalog #319198-C2), and *Slc17a7* (Mm-Slc17a7-C3; ACD, catalog #416631).

For the colocalization analysis, images (1024×1024 pixel^2) were captured with a 20× objective using an Olympus FV3000 laser-scanning confocal microscope (Olympus, Tokyo, Japan). Images were then separated into multiple color channels and cell nuclei were identified in the DAPI channel. Signals in the red, green, and magenta channels were thresholded, identified, and filtered by the locations of the nuclei. If a signal was detected in a nucleus, the cell was defined as "positive" for the respective RNA species. Nuclei positive for *Slc32a1* or *Slc17a7* were finally filtered to determine whether they co-expressed *Crhr1*.

Western blot

Mice were anesthetized with isoflurane and the mPFC were subsequently dissected and homogenized in ice-cold lysis buffer. The supernatants were obtained by centrifugation at low temperature (12,000 rpm at 4 °C for 15 min), and protein concentrations were determined using a bicinchoninic acid protein assay kit (Pierce, Rockford, IL, USA).

Samples containing 20 μg of protein were resolved on 10% sodium dodecyl sulfate-polyacrylamide gels and then transferred onto polyvinylidene difluoride membranes (Millipore, Bedford, MA, USA). The membranes were blocked with 5% non-fat milk (diluted in TBST) for 2 h at room temperature and then labeled with primary antibodies at 4 °C (overnight). The following antibodies were used: rabbit anti-CRH (1:2000, ab184238, Abcam) and mouse anti-glyceraldehyde-3-phosphate dehydrogenase (GAPDH; 1:1000, K200057M, Solarbio). After 2 h of incubation with horseradish peroxidase-conjugated secondary antibodies (1:5000, Solarbio, Beijing, China) at room temperature, the bands were visualized using an Amersham Imager 600 (GE Healthcare, PA) and analyzed using ImageJ software (NIH) by an investigator who was blinded to the treatment conditions. The values were corrected based on the levels of the corresponding control protein. The results were normalized by setting the mean value of the control group to 100%.

RNA extraction and real-time quantitative reverse transcription PCR (RT-qPCR)

Total RNA was isolated from the following target brain regions: mPFC and hippocampus using the EasyPure RNA Kit (TransGen, China). The concentration of RNA was assessed using an ND-1000 Bioanalyzer (NanoDrop, USA). The purity of total RNA was assessed by calculating the 260/280 ratio, and all samples had a ratio between 1.8 and 2.5. The RNA samples were then transcribed into cDNA using TransScript All-in-One First-Strand cDNA Synthesis SuperMix for qPCR (TransGen, China) according to the manufacturer's protocol. cDNA amplification was performed using the FastStart Essential DNA Green Master Kit (Roche, Germany) and a LightCycler® 96 real-time fluorescent quantitative PCR instrument (Roche, Germany) according to the manufacturer's standard protocols. The following primers were used for amplification:

CRH: Forward 5′- TCTCACCTTCCACCTTCTGC-3′
CRH: Reverse 5′- TTCCTGTTGCTGTGAGCTTG-3′
CRHR1: Forward 5′- TGCCAGGAGATTCTCAACGAA-3′
CRHR1: Reverse 5′- AAAGCCGAGATGAGGTTCCAG-3′
GAPDH: Forward 5′-TGTTCCTACCCCCAATGTGT- 3′
GAPDH: Reverse 5′-TGTGAGGGAGATGCTCAGTG- 3′

Reactions were run in triplicate and all samples were analyzed using the ΔΔ CT method using GAPDH as a reference gene.

CRHR1 antagonist antalarmin treatment

To investigate the intervention effects of CRHR1 blockade on the ELS negative effects, we intraperitoneally administered the CRHR1 antagonist antalarmin (20 μg/g of body weight; Sigma–Aldrich, USA) or vehicle (15% β-cyclodextrin in sterile normal saline, Solarbio, Beijing, China) in two treatment strategies. First, the concurrent blockade of CRHR1 receptors during early-life stress exposure was achieved by daily intraperitoneal injections of antalarmin or vehicle at 09:00–12:00 during PND2-8. The entire injection procedure did not exceed 10 min per cage to avoid maternal separation stress. Second, the acute pharmacological effects of antalarmin were tested in adolescent mice. In this experiment, antalarmin or vehicle was injected 30 min before behavioral tests.

Environmental enrichment

Stressed and control mice were exposed to environmental enrichment (EE) at 3–4 mice per cage from PND 22-42. The EE cage is an acrylic cage with a volume of 36 cm × 25 cm × 60 cm, divided into 3 layers (Fig. 6B). Each layer is connected by a tunnel, with facilities such as a running wheel, a swing, a pipe and a house, and toys of different shapes and colors. To ensure the novelty of the objects for the mice, the type, number, and location of the toys were changed every three days.

Quantification and statistical analysis

GraphPad Prism 9.0 (GraphPad Software, Inc., USA) was used for the statistical analyses and graphing. Signals obtained from electrophysiological recordings were analyzed with Clampfit 10.3 (Molecular Devices, Union City, CA, USA). The Kolmogorov–Smirnov test was used to assess normality before the *t*-test, ANOVA, and descriptive statistics were performed. Comparisons between the two groups were analyzed using an unpaired *t*-test (with the same variance) or an unpaired *t*-test with Welch's correction (with unequal variance). Paired *t*-tests were used to compare the percentage of time spent probing two objects in the NOR, SOR, and TOM tests. For multiple group comparisons, the data were analyzed using two-way analysis of variance (ANOVA) followed by Bonferroni's *post hoc* correction when a significant interaction was detected. Repeated measures ANOVA was used to detect the effect of ES on the frequency of evoked action potentials and VGluT1 expression on PVIs. The data are shown as individual values or presented as the mean ± SEM, and statistical significance was defined at two-sided $p < 0.05$. We did not use a method of randomization to determine samples/animals allocated to experimental groups and processed. All sample sizes, statistical methods, and results are specified in Table S2 and Table S3.

DATA AVAILABILITY

The data underlying this article will be shared on reasonable request to the corresponding author.

REFERENCES

1. Solmi M, Radua J, Olivola M, Croce E, Soardo L, de Pablo GS, et al. Age at onset of mental disorders worldwide: large-scale meta-analysis of 192 epidemiological studies. Mol Psychiatry. 2022;27:281–95.
2. Paus T, Keshavan M, Giedd JN. Why do many psychiatric disorders emerge during adolescence. Nat Rev Neurosci. 2008;9:947–57.

3. LeMoult J, Humphreys KL, Tracy A, Hoffmeister JA, Ip E, Gotlib IH. Meta-analysis: exposure to early life stress and risk for depression in childhood and adolescence. J Am Acad Child Adolesc Psychiatry. 2020;59:842–55.
4. Wade M, Wright L, Finegold KE. The effects of early life adversity on children's mental health and cognitive functioning. Transl Psychiatry. 2022;12:244.
5. Millan MJ, Agid Y, Brune M, Bullmore ET, Carter CS, Clayton NS, et al. Cognitive dysfunction in psychiatric disorders: characteristics, causes and the quest for improved therapy. Nat Rev Drug Discov. 2012;11:141–68.
6. DE Bellis MD, Hooper SR, Spratt EG, Woolley DP. Neuropsychological findings in childhood neglect and their relationships to pediatric PTSD. J Int Neuropsychol Soc. 2009;15:868–78.
7. Bath KG, Nitenson AS, Lichtman E, Lopez C, Chen W, Gallo M, et al. Early life stress leads to developmental and sex selective effects on performance in a novel object placement task. Neurobiol Stress. 2017;7:57–67.
8. Frankola KA, Flora AL, Torres AK, Grissom EM, Overstreet S, Dohanich GP. Effects of early rearing conditions on cognitive performance in prepubescent male and female rats. Neurobiol Learn Mem. 2010;94:91–99.
9. Brenhouse HC, Andersen SL. Nonsteroidal anti-inflammatory treatment prevents delayed effects of early life stress in rats. Biol Psychiatry. 2011;70:434–40.
10. Lee FS, Heimer H, Giedd JN, Lein ES, Sestan N, Weinberger DR, et al. Mental health. Adolescent mental health-opportunity and obligation. Science. 2014;346:547–9.
11. Lupien SJ, McEwen BS, Gunnar MR, Heim C. Effects of stress throughout the lifespan on the brain, behaviour and cognition. Nat. Rev. Neurosci. 2009;10:434–45.
12. Wamsley B, Fishell G. Genetic and activity-dependent mechanisms underlying interneuron diversity. Nat Rev Neurosci. 2017;18:299–309.
13. Hu H, Gan J, Jonas P. Fast-spiking, parvalbumin(+) GABAergic interneurons: from cellular design to microcircuit function. Science. 2014;345:1255263.
14. Sohal VS, Zhang F, Yizhar O, Deisseroth K. Parvalbumin neurons and gamma rhythms enhance cortical circuit performance. Nature. 2009;459:698–702.
15. Buzsaki G, Wang XJ. Mechanisms of gamma oscillations. Annu Rev Neurosci. 2012;35:203–25.
16. Canetta S, Bolkan S, Padilla-Coreano N, Song LJ, Sahn R, Harrison NL, et al. Maternal immune activation leads to selective functional deficits in offspring parvalbumin interneurons. Mol Psychiatry. 2016;21:956–68.
17. Goodwill HL, Manzano-Nieves G, LaChance P, Teramoto S, Lin S, Lopez C, et al. Early life stress drives sex-selective impairment in reversal learning by affecting parvalbumin interneurons in orbitofrontal cortex of mice. Cell Rep. 2018;25:2299–307.e2294.
18. Canetta SE, Holt ES, Benoit LJ, Teboul E, Sahyoun GM, Ogden RT et al. Mature parvalbumin interneuron function in prefrontal cortex requires activity during a postnatal sensitive period. Elife. 2022;11:e80324.
19. Patrono E, Hruzova K, Svoboda J, Stuchlík A. The role of optogenetic stimulations of parvalbumin-positive interneurons in the prefrontal cortex and the ventral hippocampus on an acute MK-801 model of schizophrenia-like cognitive inflexibility. Schizophr Res. 2023;252:198–205.
20. Caballero A, Tseng KY. GABAergic function as a limiting factor for prefrontal maturation during adolescence. Trends Neurosci. 2016;39:441–8.
21. Larsen B, Luna B. Adolescence as a neurobiological critical period for the development of higher-order cognition. Neurosci Biobehav Rev. 2018;94:179–95.
22. Sakurai T, Gamo NJ. Cognitive functions associated with developing prefrontal cortex during adolescence and developmental neuropsychiatric disorders. Neurobiol Dis. 2019;131:104322.
23. Holland FH, Ganguly P, Potter DN, Chartoff EH, Brenhouse HC. Early life stress disrupts social behavior and prefrontal cortex parvalbumin interneurons at an earlier time-point in females than in males. Neurosci Lett. 2014;566:131–6.
24. Grassi-Oliveira R, Honeycutt JA, Holland FH, Ganguly P, Brenhouse HC. Cognitive impairment effects of early life stress in adolescents can be predicted with early biomarkers: impacts of sex, experience, and cytokines. Psychoneuroendocrinology. 2016;71:19–30.
25. Ganguly P, Holland FH, Brenhouse HC. Functional uncoupling NMDAR NR2A subunit from PSD-95 in the prefrontal cortex: effects on behavioral dysfunction and parvalbumin loss after early-life stress. Neuropsychopharmacology. 2015;40:2666–75.
26. Page CE, Coutellier L. Prefrontal excitatory/inhibitory balance in stress and emotional disorders: evidence for over-inhibition. Neurosci Biobehav Rev. 2019;105:39–51.
27. Yang XD, Liao XM, Uribe-Marino A, Liu R, Xie XM, Jia J, et al. Stress during a critical postnatal period induces region-specific structural abnormalities and dysfunction of the prefrontal cortex via CRF1. Neuropsychopharmacology. 2015;40:1203–15.
28. Chen Y, Zheng Y, Yan J, Zhu C, Zeng X, Zheng S, et al. Early life stress induces different behaviors in adolescence and adulthood may related with abnormal medial prefrontal cortex excitation/inhibition balance. Front Neurosci. 2021;15:720286.
29. Pratt J, Winchester C, Dawson N, Morris B. Advancing schizophrenia drug discovery: optimizing rodent models to bridge the translational gap. Nat Rev Drug Discov. 2012;11:560–79.
30. Millan MJ, Andrieux A, Bartzokis G, Cadenhead K, Dazzan P, Fusar-Poli P, et al. Altering the course of schizophrenia: progress and perspectives. Nat. Rev Drug Discov. 2016;15:485–515.
31. Hupalo S, Bryce CA, Bangasser DA, Berridge CW, Valentino RJ, Floresco SB. Corticotropin-Releasing Factor (CRF) circuit modulation of cognition and motivation. Neurosci Biobehav Rev. 2019;103:50–59.
32. Grimm S, Gärtner M, Fuge P, Fan Y, Weigand A, Feeser M, et al. Variation in the corticotropin-releasing hormone receptor 1 (CRHR1) gene modulates age effects on working memory. J Psychiatr Res. 2015;61:57–63.
33. Davis EG, Keller J, Hallmayer J, Pankow HR, Murphy GM, Gotlib IH et al. Corticotropin-releasing factor 1 receptor haplotype and cognitive features of major depression. Transl Psychiatry. 2018;8:5.
34. Uribe-Marino A, Gassen NC, Wiesbeck MF, Balsevich G, Santarelli S, Solfrank B, et al. Prefrontal cortex corticotropin-releasing factor receptor 1 conveys acute stress-induced executive dysfunction. Biol Psychiatry. 2016;80:743–53.
35. Hupalo S, Berridge CW. Working memory impairing actions of corticotropin-releasing factor (CRF) neurotransmission in the prefrontal cortex. Neuropsychopharmacology. 2016;41:2733–40.
36. Macartney EL, Lagisz M, Nakagawa S. The relative benefits of environmental enrichment on learning and memory are greater when stressed: a meta-analysis of interactions in rodents. Neurosci Biobehav Rev. 2022;135:104554.
37. Joushi S, Esmaeilpour K, Masoumi-Ardakani Y, Esmaeili-Mahani S, Sheibani V. Effects of short environmental enrichment on early-life adversity induced cognitive alternations in adolescent rats. J Neurosci Res. 2021;99:3373–91.
38. do Prado CH, Narahari T, Holland FH, Lee HN, Murthy SK, Brenhouse HC. Effects of early adolescent environmental enrichment on cognitive dysfunction, prefrontal cortex development, and inflammatory cytokines after early life stress. Dev Psychobiol. 2016;58:482–91.
39. Liao XM, Yang XD, Jia J, Li JT, Xie XM, Su YA, et al. Blockade of corticotropin-releasing hormone receptor 1 attenuates early-life stress-induced synaptic abnormalities in the neonatal hippocampus. Hippocampus. 2014;24:528–40.
40. Liu R, Yang XD, Liao XM, Xie XM, Su YA, Li JT, et al. Early postnatal stress suppresses the developmental trajectory of hippocampal pyramidal neurons: the role of CRHR1. Brain Struct Funct. 2016;221:4525–36.
41. Wang XD, Su YA, Wagner KV, Avrabos C, Scharf SH, Hartmann J, et al. Nectin-3 links CRHR1 signaling to stress-induced memory deficits and spine loss. Nat Neurosci. 2013;16:706–13.
42. Refojo D, Schweizer M, Kuehne C, Ehrenberg S, Thoeringer C, Vogl AM, et al. Glutamatergic and dopaminergic neurons mediate anxiogenic and anxiolytic effects of CRHR1. Science. 2011;333:1903–7.
43. Zhang Q, He QY, Wang JH, Fu CY, Hu HL. Use of TAI-FISH to visualize neural ensembles activated by multiple stimuli. Nat Protoc. 2018;13:118–33.
44. Eiden LE. The vesicular neurotransmitter transporters: current perspectives and future prospects. FASEB J. 2000;14:2396–2400.
45. Wilson NR, Kang JS, Hueske EV, Leung T, Varoqui H, Murnick JG, et al. Presynaptic regulation of quantal size by the vesicular glutamate transporter VGLUT1. J Neurosci. 2005;25:6221–34.
46. van't Spijker HM, Kwok JCF. A sweet talk: the molecular systems of perineuronal nets in controlling neuronal communication. Front Integr Neurosci. 2017;11:33.
47. McBain CJ, Freund TE, Mody I. Glutamatergic synapses onto hippocampal interneurons: precision timing without lasting plasticity. Trends Neurosci. 1999;22:228–35.
48. Singec I, Knoth R, Ditter M, Volk B, Frotscher M. Neurogranin is expressed by principal cells but not interneurons in the rodent and monkey neocortex and hippocampus. J Comp Neurol. 2004;479:30–42.
49. Li JT, Xie XM, Yu JY, Sun YX, Liao XM, Wang XX, et al. Suppressed calbindin levels in hippocampal excitatory neurons mediate stress-induced memory loss. Cell Rep. 2017;21:891–900.
50. Ivy AS, Rex CS, Chen YC, Dubé C, Maras PM, Grigoriadis DE, et al. Hippocampal dysfunction and cognitive impairments provoked by chronic early-life stress involve excessive activation of CRH receptors. J Neurosci. 2010;30:13005–15.
51. Walker CD, Bath KG, Joels M, Korosi A, Larauche M, Lucassen PJ, et al. Chronic early life stress induced by limited bedding and nesting (LBN) material in rodents: critical considerations of methodology, outcomes and translational potential. Stress. 2017;20:421–48.
52. Ganguly P, Holland FH, Brenhouse HC. Functional uncoupling NMDAR NR2A subunit from PSD-95 in the prefrontal cortex: effects on behavioral dysfunction and parvalbumin loss after early-life stress. Neuropsychopharmacology. 2016;41:1188.
53. Teissier A, Le Magueresse C, Olusakin J, Andrade da Costa BLS, De Stasi AM, Bacci A et al. Early-life stress impairs postnatal oligodendrogenesis and adult emotional behaviour through activity-dependent mechanisms. Mol Psychiatry. 2019;25:1159–74.

54. Goodwill HL, Manzano-Nieves G, Gallo M, Lee HI, Oyerinde E, Serre T, et al. Early life stress leads to sex differences in development of depressive-like outcomes in a mouse model. Neuropsychopharmacology. 2019;44:711–20.
55. Molet J, Heins K, Zhuo X, Mei YT, Regev L, Baram TZ, et al. Fragmentation and high entropy of neonatal experience predict adolescent emotional outcome. Transl Psychiatry. 2016;6:e702.
56. Rincon-Cortes M, Sullivan RM. Emergence of social behavior deficit, blunted corticolimbic activity and adult depression-like behavior in a rodent model of maternal maltreatment. Transl Psychiatry. 2016;6:e930.
57. Raineki C, Cortes MR, Belnoue L, Sullivan RM. Effects of early-life abuse differ across development: infant social behavior deficits are followed by adolescent depressive-like behaviors mediated by the amygdala. J Neurosci. 2012;32:7758–65.
58. Nieves GM, Bravo M, Baskoylu S, Bath KG. Early life adversity decreases pre-adolescent fear expression by accelerating amygdala PV cell development. Elife. 2020;9:e55263.
59. Malter Cohen M, Jing D, Yang RR. Early-life stress has persistent effects on amygdala function and development in mice and humans. Proc Natl Acad Sci USA. 2013;110:18274–8.
60. Zhang Y, Sun X, Dou C, Li X, Zhang L, Qin C. Distinct neuronal excitability alterations of medial prefrontal cortex in early-life neglect model of rats. Animal Model Exp Med. 2022;5:274–80.
61. Murray AJ, Woloszynowska-Fraser MU, Ansel-Bollepalli L, Cole KL, Foggetti A, Crouch B, et al. Parvalbumin-positive interneurons of the prefrontal cortex support working memory and cognitive flexibility. Sci Rep. 2015;5:16778.
62. Cho KK, Hoch R, Lee AT, Patel T, Rubenstein JL, Sohal VS. Gamma rhythms link prefrontal interneuron dysfunction with cognitive inflexibility in Dlx5/6(+/-) mice. Neuron. 2015;85:1332–43.
63. Ferguson BR, Gao WJ. Thalamic control of cognition and social behavior via regulation of gamma-aminobutyric acidergic signaling and excitation/inhibition balance in the medial prefrontal cortex. Biol Psychiatry. 2018;83:657–69.
64. Chamberlin LA, Yang SS, McEachern EP, Lucas JTM, Ii OMW, Rolland CA, et al. Pharmacogenetic activation of parvalbumin interneurons in the prefrontal cortex rescues cognitive deficits induced by adolescent MK801 administration. Neuropsychopharmacology. 2023;48:1267–76.
65. Huang Y, Jiang H, Zheng Q, Fok AHK, Li X, Lau CG, et al. Environmental enrichment or selective activation of parvalbumin-expressing interneurons ameliorates synaptic and behavioral deficits in animal models with schizophrenia-like behaviors during adolescence. Mol Psychiatry. 2021;26:2533–52.
66. Yang YJ, Zhong ZQ, Wang BJ, Wang YL, Ding WJ. Activation of D1R signaling in the medial prefrontal cortex rescues maternal separation-induced behavioral deficits through restoration of excitatory neurotransmission. Behav Brain Res. 2023;441:114287.
67. Chocyk A, Bobula B, Dudys D, Przyborowska A, Majcher-Maslanka I, Hess G, et al. Early-life stress affects the structural and functional plasticity of the medial prefrontal cortex in adolescent rats. Eur J Neurosci. 2013;38:2089–107.
68. Hu H, Gan J, Jonas P. Interneurons. Fast-spiking, parvalbumin^{+} GABAergic interneurons: from cellular design to microcircuit function. Science. 2014;345:1255263.
69. Hijazi S, Smit AB, van Kesteren RE. Fast-spiking parvalbumin-positive interneurons in brain physiology and Alzheimer's disease. Mol Psychiatry. 2023;28:4954–67.
70. Tremblay R, Lee S, Rudy B. GABAergic interneurons in the neocortex: from cellular properties to circuits. Neuron. 2016;91:260–92.
71. Wang Y, Hu P, Shan Q, Huang C, Huang Z, Chen P, et al. Single-cell morphological characterization of CRH neurons throughout the whole mouse brain. BMC Biol. 2021;19:47.
72. Peng J, Long B, Yuan J, Peng X, Ni H, Li X, et al. A quantitative analysis of the distribution of CRH neurons in whole mouse brain. Front Neuroanat. 2017;11:63.
73. Sun QT, Li XN, Ren M, Zhao MT, Zhong QY, Ren YQ, et al. A whole-brain map of long-range inputs to GABAergic interneurons in the mouse medial prefrontal cortex. Nat Neurosci. 2019;22:1357–1370.
74. Spierling SR, Zorrilla EP. Don't stress about CRF: assessing the translational failures of CRF antagonists. Psychopharmacology. 2017;234:1467–81.
75. Sanders J, Nemeroff C. The CRF system as a therapeutic target for neuropsychiatric disorders. Trends Pharmacol Sci. 2016;37:1045–54.
76. Sun YX, Su YA, Wang Q, Zheng JY, Zhang CC, Wang T et al. The causal involvement of the BDNF-TrkB pathway in dentate gyrus in early-life stress-induced cognitive deficits in male mice. Transl Psychiatry. 2023;13:173.
77. Li Y, Shi D-D, Wang Z. Adolescent nonpharmacological interventions for early-life stress and their mechanisms. Behav Brain Res. 2023;452:114580.
78. Chen CC, Lu J, Yang R, Ding JB, Zuo Y. Selective activation of parvalbumin interneurons prevents stress-induced synapse loss and perceptual defects. Mol Psychiatry. 2018;23:1614–25.
79. Dersi G, Ozturk E, Salzberg MR, Morris M, O'Brien TJ, Jones NC. Environmental enrichment imparts disease-modifying and transgenerational effects on genetically-determined epilepsy and anxiety. Neurobiol Dis. 2016;93:129–36.
80. Sztainberg Y, Kuperman Y, Tsoory M, Lebow M, Chen A. The anxiolytic effect of environmental enrichment is mediated via amygdalar CRF receptor type 1. Mol Psychiatry. 2010;15:905–17.
81. Ma Y, Zhang C, Sun Y, Liu X, Li X-X, Wang H et al. Dorsal CA1 Nectin3 reduction mediates early-life stress-induced object recognition memory deficits in adolescent female mice. Neurosci Bull. 2024. Epub ahead of print.
82. Hippenmeyer S, Vrieseling E, Sigrist M, Portmann T, Laengle C, Ladle DR, et al. A developmental switch in the response of DRG neurons to ETS transcription factor signaling. PLoS Biol. 2005;3:e159.
83. Madisen L, Zwingman TA, Sunkin SM, Oh SW, Zariwala HA, Gu H, et al. A robust and high-throughput Cre reporting and characterization system for the whole mouse brain. Nat Neurosci. 2010;13:133–40.
84. Tsien JZ, Chen DF, Gerber D, Tom C, Mercer EH, Anderson DJ, et al. Subregion- and cell type-restricted gene knockout in mouse brain. Cell. 1996;87:1317–26.
85. Liu X, Sun YX, Zhang CC, Zhang XQ, Zhang Y, Wang T, et al. Vortioxetine attenuates the effects of early-life stress on depression-like behaviors and monoamine transporters in female mice. Neuropharmacology. 2021;186:108468.
86. Warburton EC, Brown MW. Neural circuitry for rat recognition memory. Behav Brain Res. 2015;285:131–9.
87. Cohen SJ, Stackman RW. Assessing rodent hippocampal involvement in the novel object recognition task. A review. Behav Brain Res. 2015;285:105–17.
88. Barker GRI, Warburton EC. When is the hippocampus involved in recognition memory? J Neurosci. 2011;31:10721–31.
89. Lalonde R. The neurobiological basis of spontaneous alternation. Neurosci Biobehav Rev. 2002;26:91–104.

AUTHOR CONTRIBUTIONS

TS, JL, CZ, and Y-AS designed research; YM, CY, Y-XS, C-CZ, XL, H-LW, and HW performed research; YM, CY, TW, Y-AS, X-XL, and XY analyzed data; JT, Y-AS, TS, and YM wrote the manuscript; Y-AS, JT, TS, and YM revised the manuscript.

FUNDING

This work was supported by the Beijing Natural Science Foundation (grant No., 7222236), the National Natural Science Foundation of China (grant No., 82271569, 82171529, 82071528, 82001145, 82001418, and 82371530), and the Capital's Funds for Health Improvement and Research (2022-1-4111). The funders have no role in study design, data collection and analysis, decision to publish, or preparation of the manuscript.

COMPETING INTERESTS

The authors declare no competing interests.

ETHICS APPROVAL AND CONSENT TO PARTICIPATE

All methods performed in this study were conducted in accordance with the relevant guidelines and regulations. Ethical approval was obtained from the Peking University Biomedical Ethics Committee, Laboratory Animal Welfare Ethics Sub-Committee (reference number LA2020309). Informed consent was obtained from all participants involved in the study.

ADDITIONAL INFORMATION

Supplementary information The online version contains supplementary material available at https://doi.org/10.1038/s41380-024-02845-6.

Correspondence and requests for materials should be addressed to Yun-Ai Su, Ji-Tao Li or Tian-Mei Si.